Nonminimally coupled gravitating vortex: Phase transition at critical coupling ξ_c in AdS_3

Ariel Edery*

Department of Physics and Astronomy, Bishop's University, 2600 College Street, Sherbrooke, Québec J1M 1Z7, Canada

(Received 28 June 2022; accepted 23 August 2022; published 21 September 2022)

We consider the Nielsen-Olesen vortex nonminimally coupled to Einstein gravity with a cosmological constant Λ. A nonminimal coupling term $\xi R|\phi|^2$ is natural to add to the vortex as it preserves gauge invariance (here R is the Ricci scalar and ξ a dimensionless coupling constant). This term plays a dual role: It contributes to the potential of the scalar field and to the Einstein-Hilbert term for gravity. As a consequence, the vacuum expectation value (VEV) of the scalar field and the cosmological constant in the AdS_3 background depend on ξ. This leads to a novel feature: There is a critical coupling ξ_c where the VEV is zero for $\xi \geq \xi_c$ but becomes nonzero when ξ crosses below ξ_c and the gauge symmetry is spontaneously broken. Moreover, we show that the VEV near the critical coupling has a power-law behavior proportional to $|\xi - \xi_c|^{1/2}$. Therefore, ξ_c can be viewed as the analog of the critical temperature T_c in Ginzburg-Landau (GL) mean-field theory where a second-order phase transition occurs below T_c and the order parameter has a similar power-law behavior proportional to $|T - T_c|^{1/2}$ near T_c. The plot of the VEV as a function of ξ shows a clear discontinuity in the slope at ξ_c and looks similar to plots of the order parameter versus temperature in GL theory. The critical coupling exists only in an AdS_3 background; it does not exist in asymptotically flat spacetime (topologically a cone) where the VEV remains at a fixed nonzero value independent of ξ. However, the deficit angle of the asymptotic conical spacetime depends on ξ and is no longer determined solely by the mass; remarkably, a higher mass does not necessarily yield a higher deficit angle. The equations of motion are more complicated with the nonminimal coupling term present. However, via a convenient substitution, one can reduce the number of equations and solve them numerically to obtain exact vortex solutions.

DOI: 10.1103/PhysRevD.106.065017

I. INTRODUCTION

In this work, we consider the Nielsen-Olesen vortex, a $2+1$-dimensional Abelian Higgs model, nonminimally coupled to Einstein gravity with and without a cosmological constant. Compared to previous work on the effects of gravity on vortices [1–4], the new ingredient in the action is the nonminimal coupling term $\xi R|\phi|^2$, where R is the Ricci scalar, ξ is a dimensionless coupling constant, and ϕ is a complex scalar field. When gravity is present, it is perfectly fitting to add this term to the action as it preserves the local $U(1)$ gauge invariance of the vortex.

The nonminimal coupling term changes the physical landscape significantly, in a qualitative fashion. This is related to the dual role that it plays: It acts as part of the potential for the scalar field but also contributes to the Einstein-Hilbert term for gravity. As a consequence, the old parameters when $\xi = 0$ such as the vacuum expectation value (VEV) v, cosmological constant Λ, and α (proportional to the inverse of Newton's constant) effectively become the VEV v_{eff}, the asymptotic cosmological constant Λ_{eff}, and α_{eff}, respectively, which now depend on the coupling ξ. The novel feature that emerges is that in an AdS_3 background, where Λ_{eff} is nonzero and negative, there exists a critical coupling ξ_c where the VEV v_{eff} is zero for ξ at or above ξ_c but is nonzero when ξ crosses below ξ_c. When the VEV crosses from zero to nonzero at ξ_c, the local $U(1)$ gauge symmetry is spontaneously broken corresponding to a phase transition to a vortex. The critical coupling ξ_c acts like the analog of the critical temperature T_c in Ginzburg-Landau (GL) mean-field theory where the order parameter is zero above T_c but nonzero below T_c [5,6]. There is a second-order phase transition when the temperature crosses below T_c, and this is typically accompanied by a symmetry that is spontaneously broken. The analogy between ξ_c and T_c can be made quantitative. Near ξ_c, we show that the VEV v_{eff} has a power-law behavior

*aedery@ubishops.ca

proportional to $|\xi-\xi_c|^{1/2}$ which is similar to the $|T-T_c|^{1/2}$ power-law behavior of the order parameter near T_c in GL mean-field theory [5,6]; both have a critical exponent of $1/2$. The plot of the VEV versus the coupling ξ looks very similar to the plot of the order parameter versus temperature T in GL mean-field theory, and in both cases there is a discontinuity in the slope at the critical point where the slope diverges.

The magnitude of the scalar field, represented by the function $f(r)$, starts at zero at the origin, $r=0$, and reaches its VEV asymptotically (at a large radius, the computational boundary R which formally represents infinity). An important feature is that the scalar field reaches its VEV more slowly, over a larger radius, as one approaches the critical coupling ξ_c. In other words, the core of the vortex extends out further. The plot of the scalar field's "extension"[1] as a function of ξ shows a dramatic increase near the critical coupling ξ_c. We show analytically that the extension is expected to diverge in the limit $\xi\to\xi_c$. This is the analog to the divergence of the coherence length at the critical temperature T_c in GL mean-field theory [5,6]. We also plot the extension of the magnetic field, which shows a similar trend; starting at its peak value at the origin, it falls off more slowly (extends further out) as one approaches the critical coupling ξ_c.

We derive analytical expressions for the VEV $v_{\rm eff}$ and the asymptotic cosmological constant $\Lambda_{\rm eff}$ as a function of ξ and four other parameters that appear in the Lagrangian. When $\xi=0$, $v_{\rm eff}$ reduces to v and $\Lambda_{\rm eff}$ reduces to Λ. However, when $\xi\neq 0$, $v_{\rm eff}$ does not depend only on v and ξ and $\Lambda_{\rm eff}$ does not depend only on Λ and ξ. They each depend on five parameters in total. A nonzero ξ therefore causes $v_{\rm eff}$ and $\Lambda_{\rm eff}$ to have a dependence on extra parameters besides itself compared to $\xi=0$. This wider influence ultimately stems from the aforementioned dual role that the nonminimal coupling term plays.

An important point is that the critical coupling exists only in asymptotic AdS_3 spacetime; it does not exist in asymptotically flat spacetime ($\Lambda_{\rm eff}=0$) where the VEV is a fixed nonzero constant independent of ξ. However, the nonminimal coupling term still plays a significant role in a flat background. In $2+1$-dimensional general relativity without a cosmological constant, it is well known that outside matter the spacetime is locally flat but has the topology of a cone whose deficit angle is proportional to the mass [7]. However, we find that the deficit angle is not determined solely by the mass of the vortex but also depends on the coupling ξ. One remarkable consequence of this is that a higher mass does not necessarily yield a higher deficit angle.

The focus of this paper is to study how the vortex changes with the coupling ξ. The effect of other parameters such as Λ, v, and the winding number n has already been studied in previous work [3]. We therefore fix all other parameters and obtain numerical results for different values of ξ. With the nonminimal coupling term, the equations of motion are more complicated. Nonetheless, via a convenient substitution, one can reduce the number of equations and solve them numerically. In an AdS_3 background, we obtain vortex solutions for nine values of the coupling ξ. These range from -0.14 to 0.095 (near ξ_c) and include the case $\xi=0$. For the parameters chosen, the critical coupling turns out to be equal to $\xi_c=2/21\approx 0.0952$. Note that ξ_c is an upper bound as the VEV is zero for any ξ above this value. For each ξ, we provide plots of the scalar field $f(r)$, gauge field $a(r)$, metric field $A(r)$, and magnetic field $B_m(r)$. In Table I, for each ξ, we state the numerical values obtained for the VEV $v_{\rm eff}$, the cosmological constant $\Lambda_{\rm eff}$, the ADM mass, the peak value of the magnetic field, and the numerically integrated magnetic flux. The expected theoretical values for $v_{\rm eff}$ and $\Lambda_{\rm eff}$ obtained from our derived analytical expressions are also quoted in the table. The numerical values and the theoretical expectations for the VEV, cosmological constant, and magnetic flux match almost exactly (to great accuracy, within three or four decimal places). This provides a strong mutual confirmation of both our numerical simulation and our derived analytical expressions. We verify numerically that the VEV near ξ_c indeed obeys the power law $|\xi-\xi_c|^{1/2}$. As previously mentioned, the critical exponent of $1/2$ points to a clear analogy with GL mean-field theory where ξ_c acts as the analog of the critical temperature T_c. For asymptotically flat spacetime, we consider five values of ξ ranging from -0.4 to $+0.4$. The metric field $A(r)$ starts at unity at the origin $r=0$ but then dips below unity and asymptotically reaches (at sufficiently large radius) a plateau at a positive constant value (labeled D) that is different for each ξ. This is in stark contrast to AdS_3 where the metric field $A(r)$ grows as r^2 at radius. The mass and the deficit angle at each ξ are calculated from the numerical value obtained for D.

We now place this paper in context, with a focus on previous studies of gravitating vortices that we referred to earlier [1–4]. It was recognized a long time ago that Einstein gravity in $2+1$ dimensions yields a locally flat spacetime outside localized sources, albeit with the topology of a cone [7]. However, it becomes interesting when one includes a negative cosmological constant as this leads to the famous BTZ black holes [8,9]. Later, in a higher-derivative extension of Einstein gravity in $2+1$ dimensions called Bergshoeff-Hohm-Townsend (BHT) massive gravity [10], black hole solutions in both de Sitter and anti-de Sitter space were found, as were wormhole solutions, kinks, and gravitational solitons [11]. An analytical study of black holes with spherical scalar hair in AdS_3 was later studied [1]. Closer to our topic of interest, black hole vortex solutions with a complex scalar field were constructed.

[1]The extension is defined here as the radius where it reaches 99.9% of its VEV.

These solutions departed from the conventional nonsingular vortex in two ways. The scalar field had a singularity at the origin and asymptotically tended towards zero, which satisfied the Breitenlohner-Freedman bound [12] in AdS_3 but was not the minimum of the potential. In [2], how vortices affect the tunneling decay of a false vacuum under Einstein gravity was studied, and it was found that, compared to Coleman–de Luccia bubbles [13], the tunneling exponent was less by a factor of a half. Hence, vortices are short-lived and become of cosmological interest [2]. The nonsingular vortex under Einstein gravity in an AdS_3 and Minkowski background was first studied in [3]. These were not black hole solutions as in [1]. Nonsingular vortex solutions were found numerically for different values of the cosmological constant Λ, VEV v, and winding number n. Two expressions for the (ADM) mass of the vortex were obtained: one in terms of the metric and one as an integral over purely matter fields. The latter showed that the mass was roughly proportional to n^2v^2 (an n^2 dependence was also found in [1]). The mass of the vortex increased as the magnitude of the cosmological constant increased, and this led to a slightly smaller core for the vortex. Later, work was extended to include singular vortex solutions besides nonsingular ones [4]. Vortices with conical singularities were obtained in flat backgrounds, and BTZ black hole solutions were obtained in curved backgrounds, though it was found that the vortex cannot ultimately hold a black hole at its core [4]. Our present paper introduces the nonminimal coupling term which is missing in all previous studies of gravitating vortices. As previously pointed out, this term preserves the local $U(1)$ gauge invariance of the vortex and is therefore a perfectly natural candidate to add to the action when gravity is present. We already discussed how this term significantly changes the physics qualitatively.

Our paper is organized as follows. In Sec. II, we obtain analytical expressions for the VEV v_{eff} and the cosmological constant Λ_{eff} in terms of ξ and other parameters. Details of the derivation are relegated to Appendix A. We also obtain an expression for the critical coupling ξ_c in terms of the parameters of the theory and discuss the analogy with the critical temperature T_c in GL mean-field theory. In Sec. III, we state the equations of motion in an abbreviated form, and in Appendix B we write down the full equations that are used in our numerical simulation. In Sec. IV, we obtain analytical expressions for the asymptotic metric. In Sec. V, we obtain an expression for the ADM mass as well as an expression for the deficit angle in asymptotically flat space. In Sec. VI, we state the expression for the magnetic field and derive a formula for the magnetic flux which is a topological invariant independent of ξ. In Sec. VII, we present all of our numerical results in plots and tables for different values of the coupling ξ in both an AdS_3 and a Minkowski background. Before presenting the numerical results, we obtain useful analytical expressions for the behavior of the scalar, gauge, and metric field asymptotically and near the origin. We end with our conclusion in Sec. VIII where, among other things, we discuss an interesting and challenging problem to solve in the future.

II. LAGRANGIAN FOR THE VORTEX NONMINIMALLY COUPLED TO EINSTEIN GRAVITY

The vortex nonminimally coupled to Einstein gravity with a cosmological constant has the following Lagrangian density in $2+1$ dimensions:

$$\mathcal{L} = \sqrt{-g}\left(\alpha(R-2\Lambda) - \frac{1}{4}F_{\mu\nu}F^{\mu\nu} - \frac{1}{2}(D_\mu\phi)^\dagger(D^\mu\phi) + \xi R|\phi|^2 - \frac{\lambda}{4}(|\phi|^2 - v^2)^2\right). \tag{1}$$

Here, ϕ is a complex scalar field, $F_{\mu\nu}$ is the usual electromagnetic field tensor, R is the Ricci scalar, Λ is a cosmological constant, the constant α is equal to $\frac{1}{16\pi G}$ where G is Newton's constant, and ξ is a dimensionless coupling constant. The interaction with the gauge field A_μ is incorporated via the usual covariant derivative $D_\mu\phi = \partial_\mu\phi + ieA_\mu\phi$ where e is a coupling constant. The constants λ and v are parameters that enter into the potential for the scalar field. The constants α, λ, and v are positive, whereas ξ can be positive, negative, or zero. In $2+1$-dimensional general relativity, positive Λ does not yield black holes (i.e., the famous BTZ black holes require negative Λ). Similarly, positive Λ does not support vortices [3], and the nonminimal coupling term does not change that fact. We will see that Λ must be either negative or zero, which will ultimately yield asymptotic AdS_3 or Minkowski spacetime, respectively.

The Lagrangian density has a local $U(1)$ symmetry; it is invariant under the following gauge transformations:

$$\phi(x) \to e^{ie\eta(x)}\phi(x), \tag{2}$$

$$A_\mu(x) \to A_\mu(x) - \partial_\mu\eta(x) \tag{3}$$

where $\eta(x)$ is an arbitrary function. The nonminimal coupling term $\xi R|\phi|^2$ is clearly invariant under the above gauge transformation and is therefore a perfectly natural ingredient to add to the gravitating vortex.

A. VEV and cosmological constant as a function of ξ

When $\xi = 0$, the VEV and cosmological constant are simply v and Λ, respectively. When $\xi \neq 0$, the VEV and cosmological constant change and become functions of ξ and other parameters. These will be labeled by v_{eff} and Λ_{eff} to denote that they are the actual (effective) VEV and cosmological constant, respectively, for general coupling ξ. In this

section, we determine their expressions. This requires one to know only the asymptotic behavior of the fields, and this can be determined directly from the Lagrangian without working out the full equations of motion.

Asymptotically, one reaches the vacuum when the asymptotic spacetime is either AdS_3 or Minkowski; these are maximally symmetric spacetimes that can be viewed as the ground states of general relativity [14]. In this asymptotic region, the kinetic terms for the scalar field and gauge field tend to zero: $-\frac{1}{2}(D_\mu\phi)^\dagger(D^\mu\phi) \to 0$ and $-\frac{1}{4}F_{\mu\nu}F^{\mu\nu} \to 0$. This occurs when the magnitude of the scalar field asymptotically approaches the minimum of the potential (the nonzero VEV) and the gauge field approaches a nonzero constant equal to the winding number n. In $2+1$ dimensions, the asymptotic value of the Ricci scalar is given by[2] $6\Lambda_{\rm eff}$ where $\Lambda_{\rm eff}$ is either negative (AdS_3 background) or zero (Minkowski background). The potential for the scalar field can be readily picked out from the Lagrangian and is asymptotically given by

$$\begin{aligned} V(|\phi|) &= \frac{\lambda}{4}(|\phi|^2 - v^2)^2 - \xi R|\phi|^2 \\ &= \frac{\lambda}{4}(|\phi|^2 - v^2)^2 - 6\xi\Lambda_{\rm eff}|\phi|^2. \end{aligned} \tag{4}$$

The VEV occurs at the minimum of this potential where the derivative with respect to $|\phi|$ is zero. This yields two possibilities: $|\phi| = 0$ and the solution

$$|\phi|^2 = v_{\rm eff}^2 = v^2 + \frac{12\xi\Lambda_{\rm eff}}{\lambda}. \tag{5}$$

When $v_{\rm eff}^2$ is positive, $v_{\rm eff}$ is the minimum of the potential, and it corresponds to the VEV (and $|\phi| = 0$ is a local maximum). In this case, since the VEV is nonzero, the gauge symmetry is spontaneously broken. When $v_{\rm eff}^2$ is negative (and hence $v_{\rm eff}$ is imaginary), this signals that $|\phi| = 0$ is now the minimum of the potential (the VEV). A zero VEV corresponds to the unbroken phase.

With the nonminimal coupling term $\xi R\phi^2$ present in the action, the cosmological constant is asymptotically no longer Λ but $\Lambda_{\rm eff}$; this is governed by the equation

$$\alpha(R-2\Lambda) + \xi R v_{\rm eff}^2 - \frac{\lambda}{4}(v_{\rm eff}^2 - v^2)^2 = (\alpha + v_{\rm eff}^2\xi)(R - 2\Lambda_{\rm eff}). \tag{6}$$

If we substitute $R = 6\Lambda_{\rm eff}$ above, we can solve Eqs. (5) and (6) for $v_{\rm eff}$ and $\Lambda_{\rm eff}$ as a function of ξ and the other parameters of the theory. This is worked out in Appendix A in Eqs. (A7) and (A8):

$$v_{\rm eff} = \left[2v^2 + \frac{\alpha}{\xi} - \frac{\sqrt{(\alpha + v^2\xi)^2 - 24\alpha\Lambda\xi^2/\lambda}}{\xi}\right]^{1/2} \tag{7}$$

and

$$\Lambda_{\rm eff} = \frac{\lambda}{12\xi^2}\left(\alpha + v^2\xi - \sqrt{(\alpha + v^2\xi)^2 - 24\alpha\Lambda\xi^2/\lambda}\right). \tag{8}$$

Equation (6) also implies that the coefficient in front of R asymptotically is not α but

$$\alpha_{\rm eff} = \alpha + v_{\rm eff}^2\xi. \tag{9}$$

Newton's constant is asymptotically obtained from $\alpha_{\rm eff}$, so the condition $\alpha_{\rm eff} > 0$ must be satisfied. We expect that $\lim_{\xi\to 0} v_{\rm eff} = v$, $\lim_{\xi\to 0}\Lambda_{\rm eff} = \Lambda$, and $\lim_{\xi\to 0}\alpha_{\rm eff} = \alpha$; this is in fact the case, as one can readily check. When Λ in (8) is negative, this yields a negative $\Lambda_{\rm eff}$, so the background is AdS_3. In that case, $v_{\rm eff}$ and $\Lambda_{\rm eff}$ change with ξ. However, when $\Lambda = 0$ and $\alpha + v^2\xi > 0$, one obtains $\Lambda_{\rm eff} = 0$ and $v_{\rm eff} = v$ regardless of the value of ξ or the other parameters. Therefore, in a Minkowski background ($\Lambda_{\rm eff} = 0$), the VEV remains constant at v as ξ changes. Note that $\Lambda = 0$ with $\alpha + v^2\xi < 0$ is not a physically viable option as it leads to a negative $\alpha_{\rm eff}$; i.e., one obtains $v_{\rm eff}^2 = 3v^2 + \frac{2\alpha}{\xi}$, so $\alpha_{\rm eff} = \alpha + v_{\rm eff}^2\xi$ is equal to $3(\alpha + v^2\xi)$ which is negative.

When $\xi = 0$, $v_{\rm eff}$ is simply v, but when $\xi \neq 0$, $v_{\rm eff}$ does not depend only on v, ξ, and λ but also on the gravitational parameters α and Λ. Similarly, when $\xi \neq 0$, $\Lambda_{\rm eff}$ does not depend only on Λ, ξ, and α but also on the parameters v and λ appearing in the scalar potential. We see that the nonminimal coupling term has a wide reach because of the dual role it plays in simultaneously affecting the potential of the scalar field and the Einstein-Hilbert gravitational term.

B. Critical coupling ξ_c

The VEV, given by (5), is equal to zero at a critical coupling ξ_c. This occurs when

$$2v^2 + \frac{\alpha}{\xi} - \frac{\sqrt{(\alpha + v^2\xi)^2 - 24\alpha\Lambda\xi^2/\lambda}}{\xi} = 0 \tag{10}$$

which has the solution

$$\xi_c = -\frac{2v^2\alpha\lambda}{3(v^4\lambda + 8\alpha\Lambda)} \tag{11}$$

if the condition $\alpha + 2v^2\xi > 0$ is satisfied. This condition implies that $v^4\lambda + 8\alpha\Lambda$ in the denominator of (11) is negative. The critical coupling is therefore positive and exists only when Λ is negative and obeys the inequality $\Lambda < -\frac{v^4\lambda}{8\alpha}$. A negative Λ implies $\Lambda_{\rm eff} < 0$, so the spacetime is asymptotically AdS_3. In particular, the case $\Lambda = 0$ (which yields $\Lambda_{\rm eff} = 0$) has no critical coupling and has

[2]Note that the vacuum Einstein field equations with cosmological constant $\Lambda_{\rm eff}$ yield $R = 4\Lambda_{\rm eff}$ in $3+1$ dimensions but $R = 6\Lambda_{\rm eff}$ in $2+1$ dimensions.

a fixed VEV at v. There is therefore no critical coupling in asymptotic Minkowski spacetime. The critical coupling exists only in AdS_3 when $\Lambda < -\frac{v^4\lambda}{8\alpha}$. What happens when Λ is negative but falls in the range $-\frac{v^4\lambda}{8\alpha} < \Lambda < 0$? The spacetime is asymptotically AdS_3 since $\Lambda_{\text{eff}} < 0$, and the VEV changes with ξ but it always remains above zero; there is no transition from the unbroken phase (zero VEV) to the broken phase (nonzero VEV). Note that the value of the critical coupling does not depend on the winding number n.

When the critical coupling exists, the VEV is zero for $\xi \geq \xi_c$, but it is nonzero and grows as ξ decreases below ξ_c. A phase transition from a symmetric (unbroken) phase to a spontaneously broken phase occurs when ξ crosses below ξ_c. In Fig. 1, we plot v_{eff} as a function of ξ (for parameters $\alpha = 1$, $v = 1$, $\lambda = 1$, and $\Lambda = -1$). Since $\Lambda < -\frac{v^4\lambda}{8\alpha} = -1/8$, the condition for a critical coupling is satisfied, and its value from (11) is $\xi_c = 2/21 = 0.0952$. We see that the VEV is zero above $\xi_c = 0.0952$ but becomes nonzero and increases as ξ decreases below ξ_c. The VEV is continuous, but one can readily see that the derivative (slope of the graph) is discontinuous at ξ_c. We see that, in fact, the slope diverges at that point.

Figure 1 brings to mind the graph (see Fig. 2) of the order parameter as a function of temperature in the GL mean-field theory of second-order phase transitions where the order parameter is zero above a critical temperature T_c but increases above zero below T_c. Our critical coupling ξ_c is the analog to the critical temperature T_c. We can make this connection more quantitative. In GL mean-field theory, at temperatures T below and near T_c, the order parameter is proportional to $(T_c - T)^{1/2}$ [5,6], a power-law behavior with a critical exponent of $1/2$. The VEV for ξ below and near ξ_c has a similar behavior. Using (11), we can express Λ in terms of ξ_c and substitute this into (7) to obtain

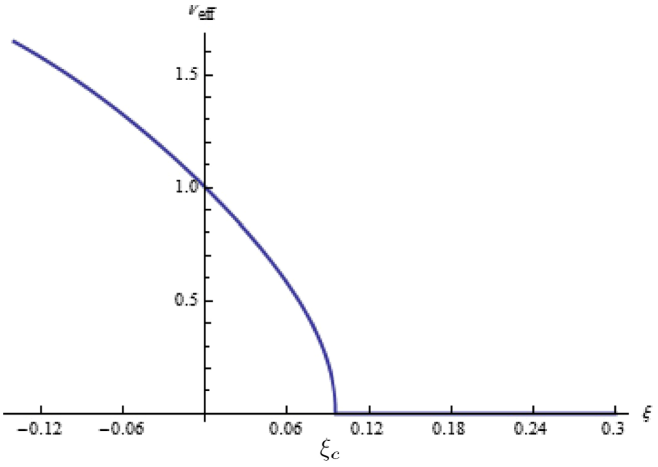

FIG. 1. VEV v_{eff} as a function of ξ plotted for parameters $\alpha = 1$, $v = 1$, $\lambda = 1$, and $\Lambda = -1$. The VEV is zero at or above $\xi_c = 0.0952$ and transitions to a nonzero value below ξ_c where it increases as ξ decreases. When ξ crosses below ξ_c, there is a transition from a symmetric phase to a spontaneously broken phase. Note that, as expected, the VEV is equal to $v = 1$ at $\xi = 0$.

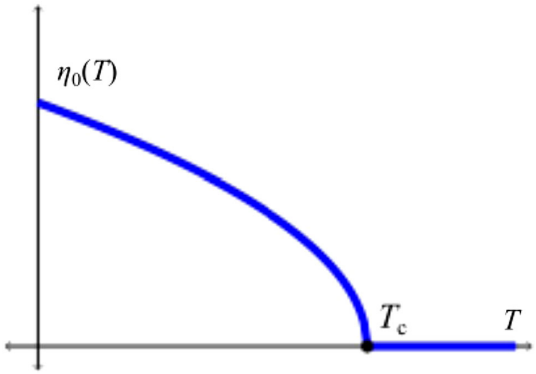

FIG. 2. Order parameter $\eta_0(T)$ as a function of temperature in the GL mean-field theory. The order parameter is zero at or above the critical temperature T_c but nonzero below T_c. There is a discontinuity in the slope at T_c, and there is a second-order phase transition when the temperature crosses below T_c. Image courtesy of C. Lygouras [15].

$$v_{\text{eff}} = \left[2v^2 + \frac{\alpha}{\xi} - \frac{\sqrt{\alpha^2 + 2v^2\alpha\xi + v^4\xi^2 - \frac{\xi^2(-2v^2\alpha\lambda - 3v^4\lambda\xi_c)}{\lambda\xi_c}}}{\xi}\right]^{1/2}. \tag{12}$$

Expanding v_{eff} above the critical coupling ξ_c yields

$$v_{\text{eff}} = k(\xi_c - \xi)^{1/2} + \mathcal{O}((\xi_c - \xi)^{3/2}) \tag{13}$$

where the proportionality constant is $k = \frac{v}{\sqrt{\xi_c + (2v^2\xi_c^2)/\alpha}}$. We therefore see that the power-law behavior of the VEV near ξ_c and of the order parameter near T_c in GL theory is similar and has the same critical exponent of $1/2$. From (13), one can readily see that the slope in Fig. 1 diverges at ξ_c (just like the slope in Fig. 2 diverges at T_c). We see that the VEV for values of ξ near ξ_c in our numerical simulation closely follows the power-law behavior given by (13).

We now determine the equations of motion, solve them numerically, and obtain plots of various quantities for different values of the coupling ξ. Equations (7) and (8) for the VEV and cosmological constant that we derived in this section will be used to predict the asymptotic values of our plots, and we will see that they match exactly. This provides a strong confirmation of both our derived theoretical results in this section and of our numerical vortex solutions in later sections.

III. ROTATIONALLY SYMMETRIC ANSATZ AND EQUATIONS OF MOTION

For the vortex, we consider rotationally symmetric static solutions. The ansatz for the gauge and scalar field is

$$A_j(\mathbf{x}) = \epsilon_{jk}\hat{x}^k \frac{a(r)}{er}, \tag{14}$$

$$\phi(\mathbf{x}) = f(r)e^{in\theta} \tag{15}$$

where $a(r)$ and $f(r)$ are functions of r that represent the gauge and scalar fields, respectively. The non-negative integer n is called the winding number. A $2+1$-dimensional metric that is rotationally symmetric can be expressed as

$$ds^2 = -B(r)dt^2 + \frac{1}{A(r)}dr^2 + r^2 d\theta^2 \tag{16}$$

where $A(r)$ and $B(r)$ represent two metric functions of r.

With the ansatz (15) and (16), the Langrangian density (1) reduces to

$$\mathcal{L} = \sqrt{B/A}r\bigg(\alpha(R-2\Lambda) - \frac{A(a')^2}{2e^2r^2} - \frac{(f')^2A}{2} - \frac{(n-a)^2f^2}{2r^2} + \xi R f^2 - \frac{\lambda}{4}(f^2-v^2)^2\bigg). \tag{17}$$

Since f approaches a nonzero constant asymptotically, one requires that $a \to n$ asymptotically [which yields $(n-a)^2f^2 \to 0$] so that one avoids a logarithmic divergence in the energy of the vortex [3,16]. The Ricci scalar is a function of A and B and their derivatives:

$$R = \frac{(B')^2A}{2B^2} - \frac{A'}{r} - \frac{A'B'}{2B} - \frac{B'A}{rB} - \frac{B''A}{B}. \tag{18}$$

Note that when the complex scalar field is inserted in the Lagrangian density, the winding number n appears but not the coordinate θ since the phase cancels out. The Lagrangian density therefore depends on r only, and solutions are rotationally symmetric. The Euler-Lagrange equations of motion for $A(r)$, $B(r)$, $f(r)$, and $a(r)$ are, respectively,

$$4e^2rAB'(\alpha+\xi f^2+2r\xi ff') + B(e^2r^2(v^4\lambda+8\alpha\Lambda) + 2e^2(n^2-r^2v^2\lambda-2na+a^2)f^2 + e^2r^2\lambda f^4 + 16e^2r\xi Aff' - 2A(a'^2+e^2r^2f'^2)) = 0, \tag{19}$$

$$e^2r^2\lambda f^4 + e^2r(rv^4\lambda + 8r\alpha\Lambda + 4\alpha A') + 2e^2f^2(n^2 - r^2v^2\lambda - 2na + a^2 + 2r\xi A') + 2A(a'^2 + e^2r^2(1+8\xi)f'^2) + 8e^2r\xi f(rA'f' + 2A(f' + rf'')) = 0, \tag{20}$$

$$2r^2\xi AfB'^2 + rB(-2r\xi fA'B' + A(rB'f' - 4\xi f(B' + rB''))) + B^2(-2r^2\lambda f^3 - 2f(n^2 - r^2v^2\lambda - 2na + a^2 + 2r\xi A') + r(rA'f' + 2A(f' + rf''))) = 0, \tag{21}$$

$$rAa'B' + B(2e^2r(n-a)f^2 - 2Aa' + ra'A' + 2rAa'') = 0. \tag{22}$$

We can reduce the above four equations of motion to three by extracting $W(r) = B'/B$ from Eq. (19) and substituting it into Eqs. (21) and (22). The function $W(r)$ contains A, f, and a and their derivatives. The main point is that the three remaining equations no longer have any dependence on $B(r)$. However, the equations become longer, especially the one for the function $f(r)$. We write out the full equations in Appendix B; Eqs. (B2)–(B4) are the equations we solve numerically. To avoid writing out cumbersome lengthy equations here, the three remaining equations are written below using $W(r)$ and $W'(r)$. Note that we need W' because of the appearance of B'' in (21). In particular, $B''/B = W' + W^2$. The three remaining equations are

$$e^2r^2\lambda f^4 + e^2r(rv^4\lambda + 8r\alpha\Lambda + 4\alpha A') + 2e^2f^2(n^2 - r^2v^2\lambda - 2na + a^2 + 2r\xi A') + 2A(a'^2 + e^2r^2(1+8\xi)f'^2) + 8e^2r\xi f(rA'f' + 2A(f' + rf'')) = 0, \tag{23}$$

$$2r^2\xi AfW^2 - 2r^2\xi fA'W + Ar(rWf' - 4\xi f(W + r(W' + W^2))) - 2r^2\lambda f^3 - 2f(n^2 - r^2v^2\lambda - 2na + a^2 + 2r\xi A') + r(rA'f' + 2A(f' + rf'')) = 0, \tag{24}$$

$$rAa'W + 2e^2r(n-a)f^2 - 2Aa' + ra'A' + 2rAa'' = 0. \tag{25}$$

When $W(r)$ given by (B1) is substituted into the above equations, we obtain Eqs. (B2)–(B4).

IV. ASYMPTOTIC ANALYTICAL SOLUTIONS

One can solve analytically for the metric in vacuum by setting $f = v_{\rm eff}$ and $a = n$ identically in Eq. (23). This yields

$$A'(r) = -r\frac{(8\alpha\Lambda + \lambda(v_{\rm eff}^2 - v^2)^2)}{4(\alpha + \xi v_{\rm eff}^2)} \tag{26}$$

with the solution

$$A_0(r) = -\frac{(8\alpha\Lambda + \lambda(v_{\rm eff}^2 - v^2)^2)}{8(\alpha + \xi v_{\rm eff}^2)}r^2 + C = -\Lambda_{\rm eff}r^2 + C \tag{27}$$

where the subscript "0" denotes vacuum and C is an integration constant. In the last step, we substituted $v_{\rm eff}$ given by (7), and this yields $\Lambda_{\rm eff}$ given by (8) as the coefficient of $-r^2$ [see also Eq. (A3)]. Of course, this is exactly what we expect the metric of pure AdS_3 to be for the cosmological constant $\Lambda_{\rm eff}$. The initial conditions at $r = 0$ are determined by the constant C. We set $C = 1$ since in $2+1$ dimensions this choice avoids a conical singularity

at the origin [7,8]. Moreover, $C = 1$ also works for the case of vortices embedded in asymptotically Minkowski spacetime ($\Lambda_{\text{eff}} = 0$).

We can now solve for the metric function $B_0(r)$ in vacuum by substituting $A_0(r)$ with $C = 1$ into Eq. (19). This yields $B_0(r) = k_0(-\Lambda_{\text{eff}} r^2 + 1)$ where k_0 is an integration constant (positive). We can absorb this constant into a redefinition of time in the line element (16) so that

$$B_0(r) = -\Lambda_{\text{eff}} r^2 + C = A_0(r). \tag{28}$$

In the presence of the vortex, we have that $f \to v_{\text{eff}}$ and $a \to n$ asymptotically. Note that in contrast to the vacuum case, these are now only the asymptotic values. The vortex departs significantly from that in the core region near the origin. In numerical simulations, f and a start at zero at the origin and reach their asymptotic values (within less than a percent) at a finite radius R, the computational boundary which formally represents infinity. The asymptotic form of the metric function A in the presence of matter (the vortex) is obtained again via Eq. (23) and yields, at $r = R$,

$$A(R) = -\Lambda_{\text{eff}} R^2 + D. \tag{29}$$

The constant D differs from the constant C in (27); as one goes through the core of the vortex, one naturally emerges into an asymptotic region that differs from the purely vacuum one, and this is reflected in D being a different constant from C. We see that the (ADM) mass of the vortex is expressed in terms of $A_0(R)$ and $A(R)$.

Asymptotically, using (19), we obtain $B(R) = kA(R)$. Here k is an integration constant (positive); it can no longer be absorbed into a redefinition of time since this has been carried out once already with the constant k_0. At large radius R, in the presence of the vortex, we obtain that $B(R)$ is proportional to $A(R)$ but not equal to it.

V. EXPRESSION FOR THE (ADM) MASS OF THE VORTEX

An important property of a vortex is its finite mass. In curved spacetime, the mass of a localized source is defined as its ADM mass [17]. AdS_3 is a maximally symmetric spacetime with isometry group $SO(2,2)$; it has a timelike Killing vector, so a conserved energy (the ADM mass) naturally applies to matter embedded in it. The ADM mass in $2+1$ dimensions can be calculated via the following expression [17]:

$$M = -2\alpha_{\text{eff}} \lim_{C_t \to R} \oint_{C_t} (k - k_0)\sqrt{\sigma} N(R) d\theta. \tag{30}$$

Note that α_{eff}, given by (9), must be used here instead of α. Here C_t is the circle at spatial infinity where infinity corresponds to the computational boundary $r = R$. The lapse $N(R)$ is given by $(B_0(R))^{1/2} = (A_0(R))^{1/2}$. The metric on C_t is σ_{AB}, and $\sqrt{\sigma} = R$ where σ is its determinant. The extrinsic curvature of C_t embedded in the two-dimensional spatial surface obtained by setting t constant in (16) is given by k, whereas its embedding in the two-dimensional spatial surface of AdS_3 is given by k_0. A straightforward calculation yields

$$k = \frac{(A(R))^{1/2}}{R}, \qquad k_0 = \frac{(A_0(R))^{1/2}}{R}. \tag{31}$$

Substituting all of the above quantities into (30) yields our final expression for the ADM mass:

$$M = 4\pi\alpha_{\text{eff}}(A_0(R) - [A_0(R)A(R)]^{1/2}). \tag{32}$$

We use the above expression to calculate the ADM mass in an AdS_3 background. Note that if $A(R) = A_0(R)$, one obtains $M = 0$, which implies that our definition has set empty AdS_3 space to have zero mass. This is the desired and expected result since maximally symmetric spacetimes can be viewed as the ground states of general relativity [14] and, as such, are typically set to zero energy.

The analytical expression (27) for the vacuum metric $A_0(R)$ is $-\Lambda_{\text{eff}} R^2 + 1$, and this can be readily calculated for any given R. From (29), we have that $A(R) = -\Lambda_{\text{eff}} R^2 + D$ where D is a constant. This corresponds to the case with matter (the vortex), and it is obtained by solving the equations of motion numerically since we do not know *a priori* the value of the constant D. The mass M of the vortex is then obtained via (32). Though $A_0(R)$ and $A(R)$ both change with R, at a large enough R, the mass M hardly changes as R increases and the matter fields $f(r)$ and $a(r)$ plateau to their respective asymptotic values of v_{eff} and n. The value of $A(r)$ at $r = 0$ is an initial condition. In vacuum, $A(r)$ must reduce to $A_0(r)$ so that the initial conditions at the origin match. This implies that $A(0) = A_0(0) = C = 1$.

A. ADM mass in asymptotically flat space and angular deficit

In asymptotically flat spacetime where $\Lambda = \Lambda_{\text{eff}} = 0$, the ADM mass formula (32) remains valid but simplifies greatly. We have that $A_0(R) = C = 1$ and $A(R) = D$ which yields

$$M_{\text{flat}} = 4\pi\alpha_{\text{eff}}(1 - D^{1/2}) \tag{33}$$

where $\alpha_{\text{eff}} = \alpha + \xi v^2$ since $v_{\text{eff}} = v$. Note that $A_0(r) = B_0(r)$ stays constant at unity for all r (this represents the vacuum Minkowski spacetime). In contrast, $A(r)$ is unity at the origin $r = 0$ but dips below unity as r increases until it plateaus to a positive value D at large radius R. The value of D is obtained numerically. Recall that localized matter in $2+1$ dimensions yields an asymptotically Minkowski spacetime with an angular deficit [7]. Asymptotically,

$A(r) = D$, and the spatial part of the metric (16) becomes $\frac{dr^2}{D} + r^2 d\theta^2$. If we define $r_0 = r/D^{1/2}$ and $\theta_0 = D^{1/2}\theta$, we obtain a manifestly flat metric $dr_0^2 + r_0^2 d\theta_0^2$ but with θ_0 now ranging from 0 to $2\pi D^{1/2}$ instead of 2π. Since $0 < D < 1$, there is an angular deficit of

$$\delta = 2\pi(1 - D^{1/2}). \tag{34}$$

Using (33) with $\alpha_{\rm eff} = 1/(16\pi G_{\rm eff})$, we obtain that $\delta = 8\pi G_{\rm eff} M_{\rm flat}$, which is the formula for the angular deficit produced by a mass $M_{\rm flat}$ in $2+1$ Minkowski spacetime [7] if $G_{\rm eff}$ replaces G in [7]. Asymptotically, the spacetime is locally flat but topologically a cone. However, there is no conical singularity at the origin in our case, in contrast to the point mass in [7]. The spacetime is smooth at the origin since the vortex, by construction, is an extended nonsingular object. In our case, the conical spacetime is only the asymptotic spacetime, and it does not extend into the core of the vortex.

In the original work of [7], the only way to change the angular deficit is to change the mass since G remains constant. In our case, $G_{\rm eff}$ depends on the coupling ξ. Therefore, as ξ changes, one can encounter a scenario (and one does, as our numerical results will show) where a higher mass yields a smaller deficit angle than a smaller mass. This is another instance of how the nonminimal coupling term plays a novel role.

VI. MAGNETIC FLUX AS A TOPOLOGICAL INVARIANT INDEPENDENT OF COUPLING ξ

The vortex contains a magnetic field which we label B_m. When we plot our numerical results, we will see that it has its maximum at the origin and then decreases towards zero outside a core region. The maximum value of the magnetic field at the origin, as well as its profile, depends on the coupling ξ. After we present our numerical results, we will look at the radial extension of the scalar field as a function of ξ, a measure of how far the field extends before it gets close to its plateau value (the VEV). We will see that the radial extension of the scalar field increases significantly as we approach the critical coupling ξ_c. This is analogous to the coherence length in GL mean-field theory which diverges near the critical temperature. We discuss here the radial extension of the scalar field because we see that the radial extension of the magnetic field as a function of ξ undergoes the same fate and also increases as we approach the critical coupling ξ_c. The magnetic field profile therefore provides us with an additional window into how far the core region of the vortex extends.

An important property of the magnetic field is that even though its profile changes with the coupling ξ, the magnetic flux Φ obtained by integrating the magnetic field over the entire two-dimensional area stays constant (i.e., it is independent of the value of ξ). We show here that the magnetic flux depends only on the winding number n and hence is a topological invariant. The quantity $-\frac{A(a')^2}{2e^2r^2}$ appearing in the Lagrangian density (17) stems from the term $-\frac{1}{4}F_{\mu\nu}F^{\mu\nu}$ and hence is identified with $-B_m^2/2$ where B_m is the magnetic field (no electric field is present, hence the absence of an $\frac{E^2}{2}$ term). It follows that the magnetic field is given by $B_m = \frac{\sqrt{A}a'}{er}$ which reduces to the well-known result $a'/(er)$ for the magnetic field in fixed Minkowski spacetime [16] where $A(r) = 1$ identically.

The magnetic flux Φ, the integral of the magnetic field over the invariant area element, yields

$$\begin{aligned}\Phi &= \int d^2x\sqrt{\gamma}B_m = \int dr d\theta \left(\frac{r}{\sqrt{A}}\right)\left(\frac{\sqrt{A}a'}{er}\right) \\ &= \frac{2\pi}{e}\int_0^R a' dr = \frac{2\pi}{e}(a(R) - a(0)) = \frac{2\pi n}{e}\end{aligned} \tag{35}$$

where $\gamma = r^2/A$ is the determinant of the spatial two-metric obtained from (16) by setting t constant. We use the boundary conditions on the function $a(r)$: $a(R) = n$ and $a(0) = 0$. Note that the expression for the magnetic flux $\Phi = \frac{2\pi n}{e}$ is the same in curved space as it is in fixed Minkowski spacetime [16]. In the next section, where we present our numerical results, we will integrate numerically over the area of the different magnetic field profiles for different couplings ξ and show that the result is the same, independent of the profile and ξ. Besides demonstrating numerically that the magnetic flux is a topological invariant in curved space, this also provides another check on our numerical simulation. The magnetic flux is "quantized" as it comes in integer steps of $2\pi/e$. This does not stem from any quantization procedure imposed on the fields but from the topology of the vortex, which is characterized by its winding number n.

VII. NUMERICAL SOLUTIONS OF VORTEX IN CURVED SPACE

The three equations of motion, Eqs. (B2)–(B4), are solved numerically to obtain nonsingular profiles for the scalar field $f(r)$, the gauge field $a(r)$, and the metric function $A(r)$. The initial conditions at the origin $r = 0$ are

$$f(0) = 0, \qquad a(0) = 0, \qquad A(0) = 1. \tag{36}$$

These initial conditions ensure that our vortex solutions are nonsingular. Let R be the computational boundary formally representing infinity. We expect that

$$f(R) = v_{\rm eff}, \qquad a(R) = n, \qquad A(R) = D - \Lambda_{\rm eff}R^2 \tag{37}$$

where D is a constant that is determined only after running the numerical simulation and it depends on the matter distribution of the vortex. The quantity $v_{\rm eff}$ is the value where $f(r)$ plateaus numerically, and we see that it matches

very closely our theoretical prediction given by (7). The winding number of the vortex is given by the positive integer n, and we see that $a(r)$ plateaus at that value numerically. The coefficient Λ_{eff} in front of R^2 in $A(R)$ can be extracted from our numerical simulation by evaluating $-A''(r)/2$ at $r = R$. We see that it matches very closely our theoretical prediction for the asymptotic value of the cosmological constant given by (8). We obtain the profiles

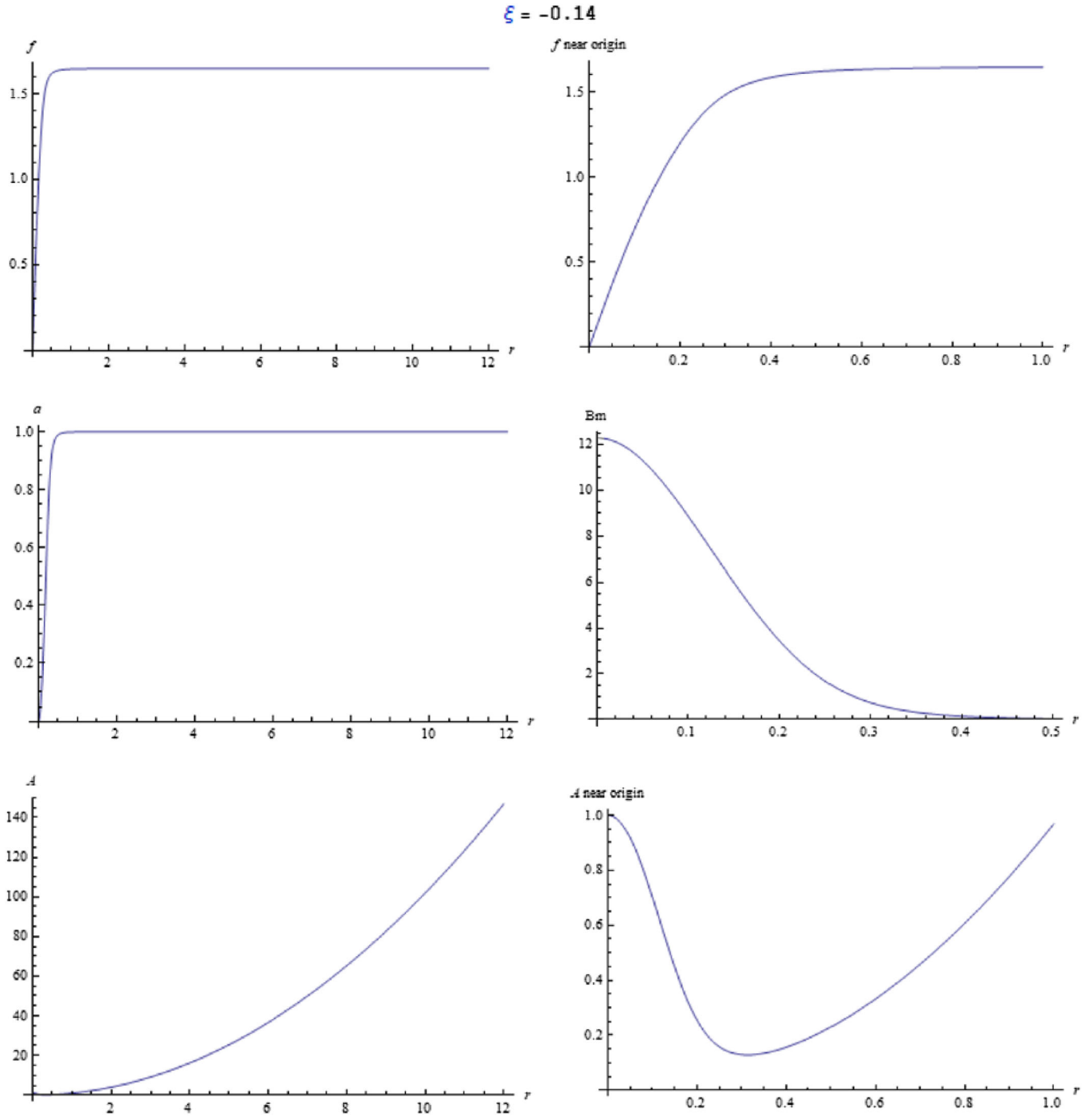

FIG. 3. Case $\xi = -0.14$. This is the case with the lowest value of ξ and the highest VEV (value where f plateaus). The gauge field plateaus at $n = 1$ which is the same value for all subsequent cases. The dip in the metric function $A(r)$ near the origin is the most pronounced of our sample. The magnetic field B_m peaks at the origin and has the highest peak in our sample. The magnetic field also falls off the fastest (extends out the least). The plot of f near the origin shows that f plateaus quickly (does not extend much before reaching its VEV).

by adjusting $f'(r)$ and $a'(r)$ near the origin until the curves for $f(r)$ and $a(r)$ plateau towards their respective constant values beyond a certain radius (in our numerical simulations, they reach their expected constant values to within less than a tenth of a percent at the computational boundary R).

A. Analytical behavior of the fields asymptotically and near the origin

The equations of motion are a long, complicated set of coupled, nonlinear, differential equations which require a numerical solution. However, before presenting the numerical results, it is instructive to extract some useful analytical

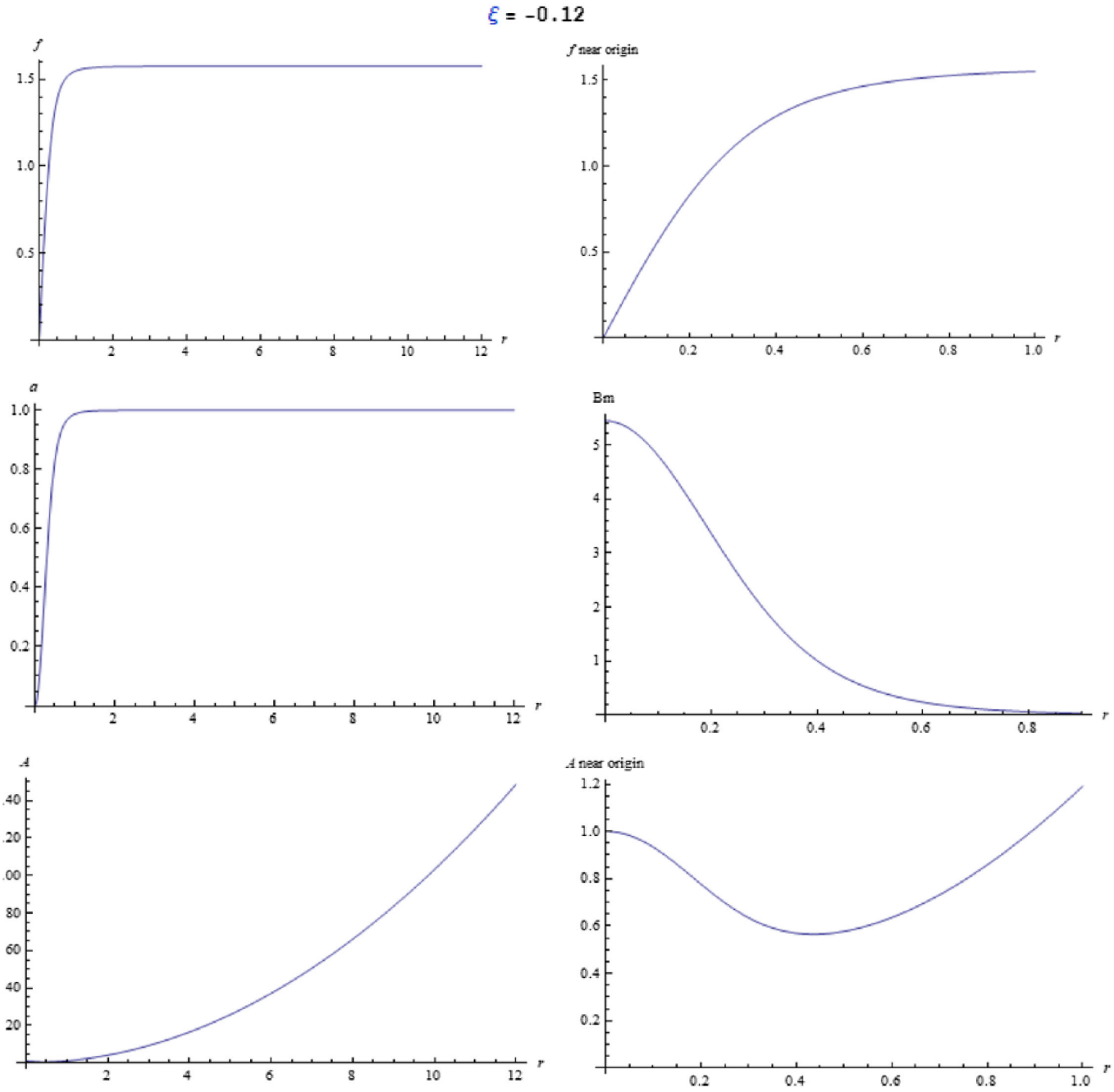

FIG. 4. Case $\xi = -0.12$. This is the case with the next lowest value of ξ. Note that f plateaus at a lower VEV than $\xi = -0.14$, but it has the highest (ADM) mass in our sample. The dip in the metric function $A(r)$ near the origin is not as pronounced as in $\xi = -0.14$. The magnetic field B_m at the origin is lower than for $\xi = -0.14$, but it falls off more slowly so that the magnetic flux turns out to be the same. Again, the plot of f near the origin shows that f plateaus quickly and hence has a small extension.

information from the equations. In particular, we determine the analytical behavior of the fields near the origin and in the asymptotic region. We see that the asymptotic profile of a vortex is not supported by a positive cosmological constant Λ_{eff}; it must be either negative (AdS_3 background) or zero (Minkowski background). This is similar to the fact that in $2+1$-dimensional general relativity, a black hole exists for a negative cosmological constant (the BTZ black hole [8,9]) but not for a positive cosmological constant. There is no black hole in a Minkowski background either, but in contrast, one can have a vortex in a Minkowski background.

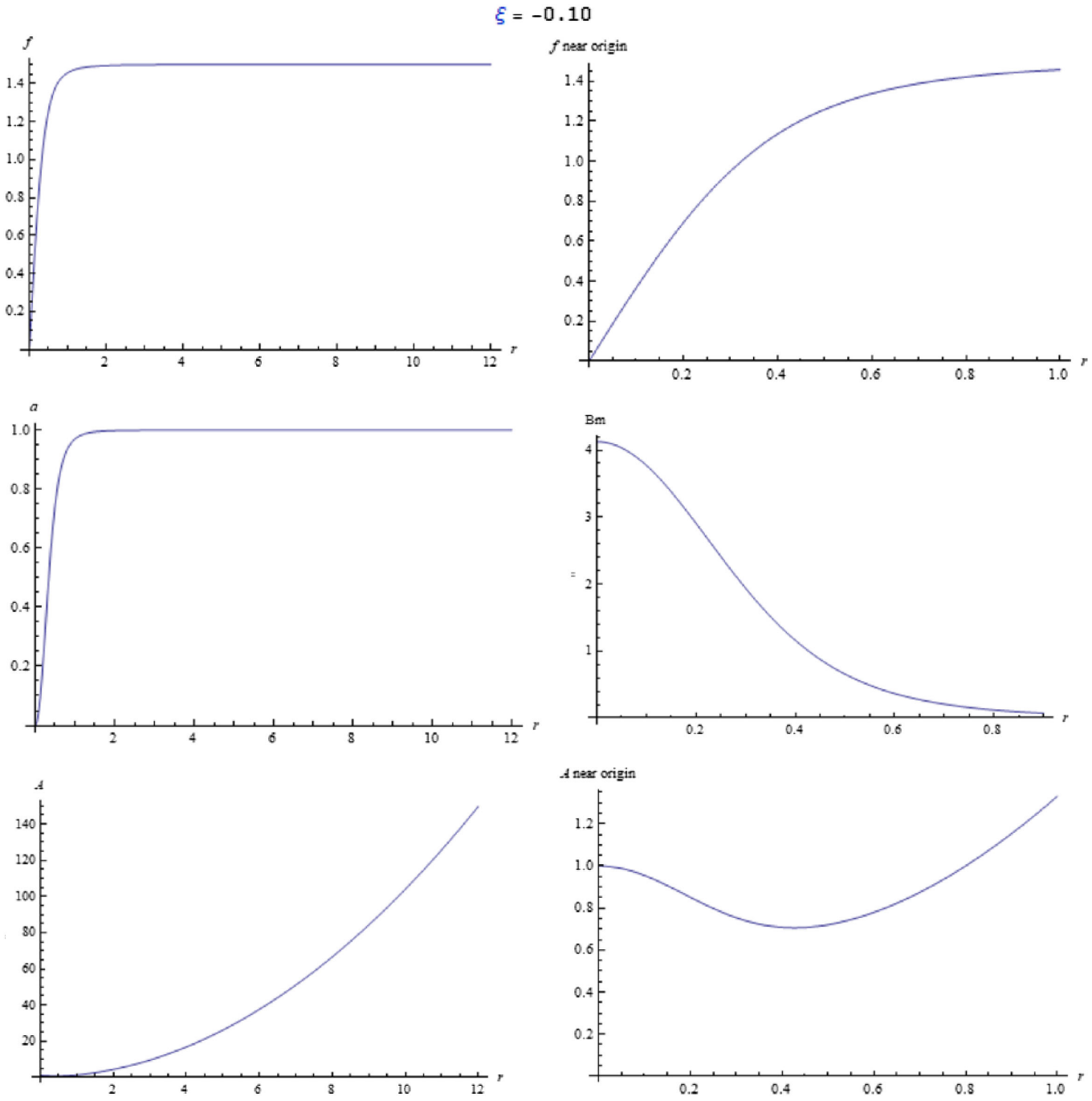

FIG. 5. Case $\xi = -0.10$. Note that f plateaus at a lower VEV than the previous cases. The dip in the metric function $A(r)$ near the origin is still pronounced but not as much as in $\xi = -0.12$ or $\xi = -0.14$. The magnetic field B_m at the origin is lower than for $\xi = -0.12$, but it falls off more slowly, which yields the same magnetic flux as previous cases. The plot of f near the origin shows that f still plateaus relatively quickly though less fast than in previous cases.

1. Behavior of $A(r)$, $f(r)$, and $a(r)$ near the origin

The initial conditions on the fields at $r = 0$ are $f(0) = 0$, $a(0) = 0$, and $A(0) = 1$. We want to find the behavior of these fields in the vicinity of $r = 0$. If we linearize (B2) about $A = 1$, we obtain $A(r) = 1 - r^2(\frac{v^4\lambda}{8\alpha} + \Lambda)$. This quadratic behavior implies that its first derivative $A'(r)$ at $r = 0$ is always zero regardless of the parameters, so the metric function always starts out flat at the origin. This is what is observed numerically. Linearizing (B4) about $a = 0$ yields $a(r) = br^2$ with b a positive constant. We see that $a(r)$ also starts out flat at the origin since $a'(0) = 0$. Again, this agrees with our numerical simulation.

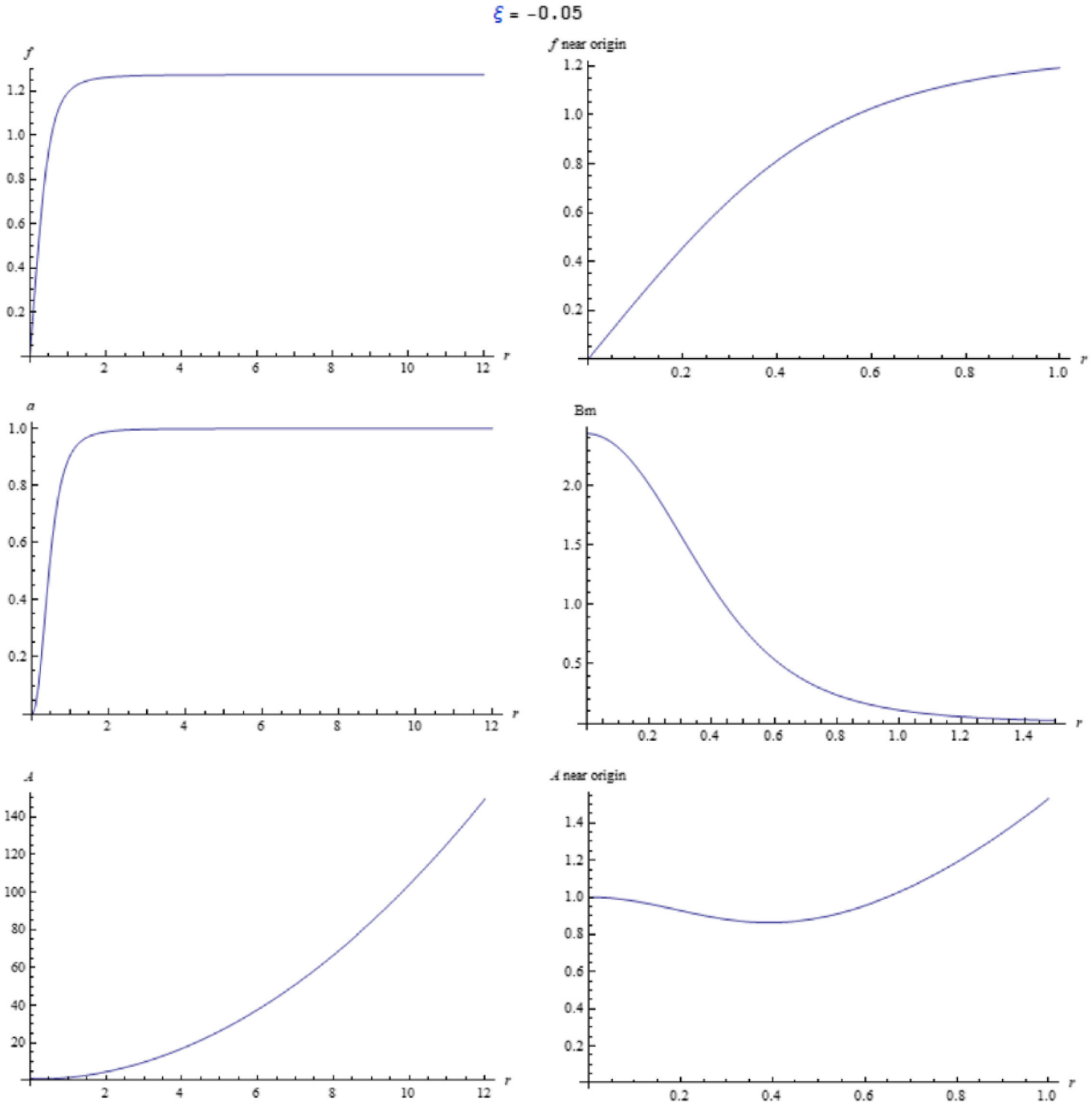

FIG. 6. Case $\xi = -0.05$. Note that f plateaus at a lower VEV than the previous cases. The dip in the metric function $A(r)$ near the origin is visible but not as pronounced as in previous cases. The magnetic field B_m has a profile that yields the same magnetic flux as previous cases. The plot of f near the origin now shows that f is no longer plateauing quickly (it needs to extend more before reaching its VEV).

Linearizing (B3) about $f = 0$ yields $f(r) = cr^n$ where n is the winding number and c a positive constant. Near the origin, $f'(r) = cnr^{n-1}$ so that $f'(0) = c$ for $n = 1$ and $f'(0) = 0$ for $n > 1$. This implies that $f(r)$ starts off flat at the origin when $n > 1$ but with a positive slope when $n = 1$. Note that the fields near $r = 0$ have no dependence on the coupling ξ.

2. Behavior of $A(r)$, $f(r)$, and $a(r)$ asymptotically

Asymptotically, the metric function $A(r)$ is given by $D - \Lambda_{\text{eff}} r^2$ where D is a constant. The matter fields a and f asymptotically plateau to their constant values of n and v_{eff}, respectively. We want to find their behavior as they approach these constant values. At large r, we can write $a(r) = n - \epsilon(r)$ and $f(r) = v_{\text{eff}} - \beta(r)$ where ϵ and β are

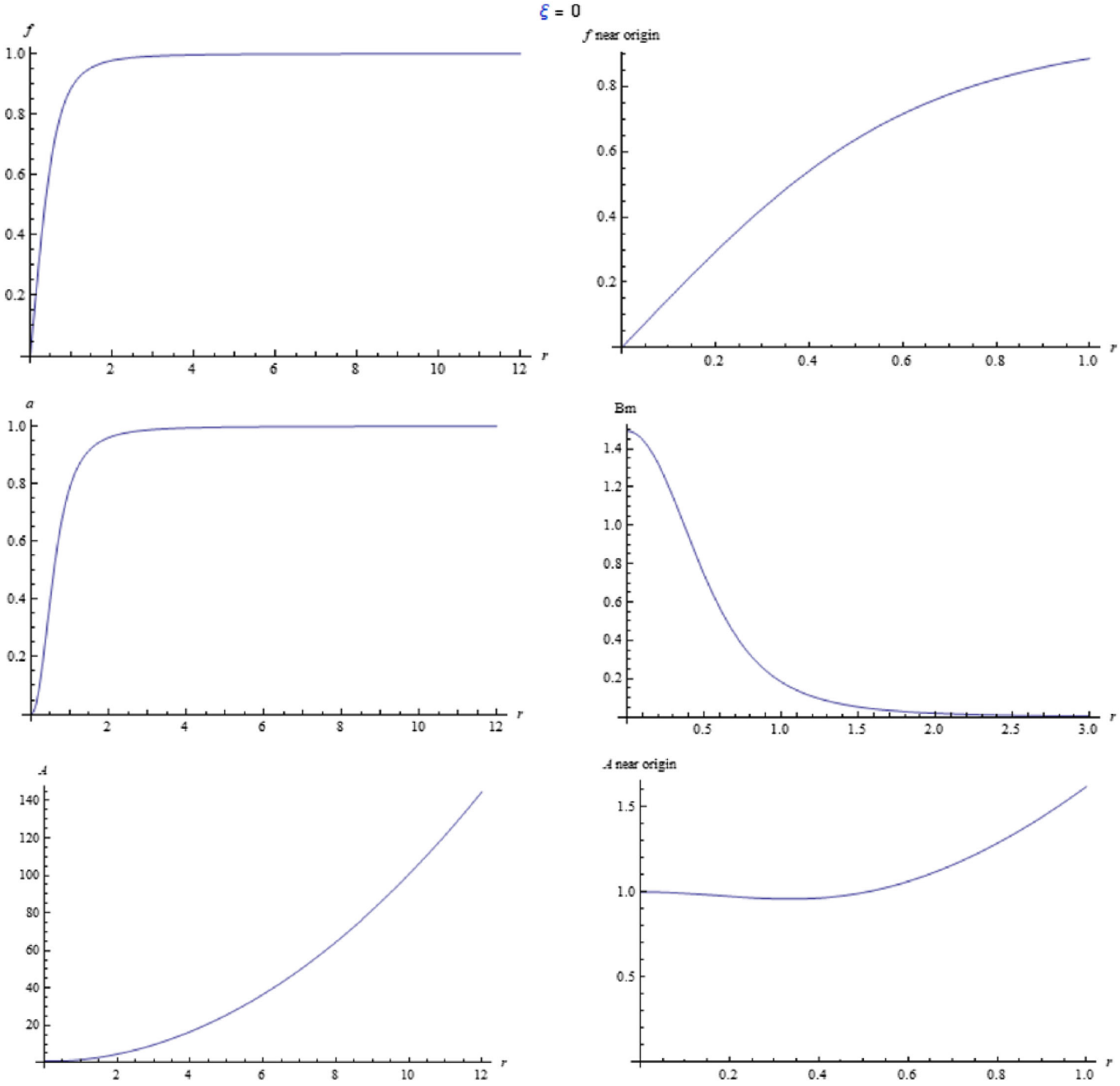

FIG. 7. Case $\xi = 0$. The nonminimal coupling term is turned off. The VEV is therefore equal to $v = 1$. The dip in the metric function $A(r)$ near the origin is still visible. The magnetic field B_m extends further out but yields the same magnetic flux as previous cases. The plot of f near the origin shows that f is still rising and requires more radial distance before it plateaus to its VEV.

small positive perturbations which must vanish asymptotically. Substituting these expressions into Eqs. (B4) and (B3) and keeping only terms linear in ϵ and β yields the differential equations

$$e^2 v_{\rm eff}^2 \epsilon(r) + r\Lambda_{\rm eff}\epsilon'(r) + r^2\Lambda_{\rm eff}\epsilon''(r) = 0, \quad (38)$$

$$2v_{\rm eff}^2(\alpha_{\rm eff}\lambda - 24\Lambda_{\rm eff}\xi^2)\beta(r) + r\Lambda_{\rm eff}(\alpha_{\rm eff} + 16v_{\rm eff}^2\xi^2)(3\beta'(r) + r\beta''(r)) = 0. \quad (39)$$

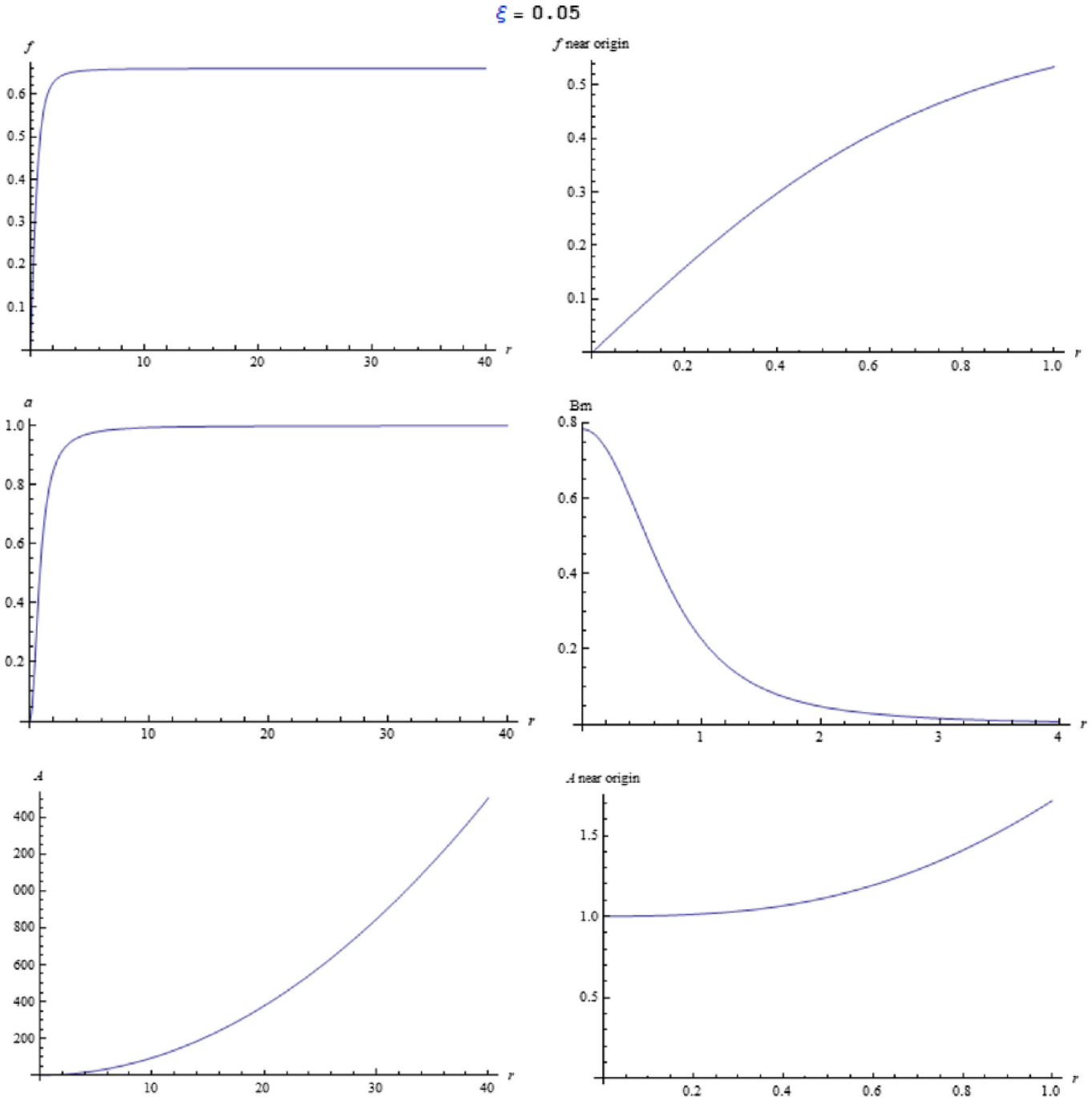

FIG. 8. Case $\xi = 0.05$. The regular plot of f vs r now has a computational boundary of $R = 40$ whereas in all previous cases it was $R = 12$. This is because f reaches its VEV now much more slowly, and one needs to extend the computational boundary so that f can reach its VEV to the same level of accuracy. The plot of f near the origin shows that f has a large slope and is also far from its plateau value; thus, it requires significantly more radial distance before it plateaus to its VEV. The numerical values of the metric function A show that there is an extremely tiny dip right near the origin, but this is not visible on the plot. The magnetic field B_m, just like f, extends further out than all previous cases.

The above equations are valid only for the case $\Lambda_{\text{eff}} \neq 0$ (the case $\Lambda_{\text{eff}} = 0$ will be treated separately). Both equations have power-law falloff solutions

$$\epsilon(r) = br^{-\frac{er_{\text{eff}}}{(-\Lambda_{\text{eff}})^{1/2}}}, \tag{40}$$

$$\beta(r) = cr^{-1-\left[\frac{-\alpha_{\text{eff}}\Lambda_{\text{eff}}+2\alpha_{\text{eff}}v_{\text{eff}}^2\lambda-64v_{\text{eff}}^2\Lambda_{\text{eff}}\xi^2}{-\alpha_{\text{eff}}\Lambda_{\text{eff}}-16v_{\text{eff}}^2\Lambda_{\text{eff}}\xi^2}\right]^{1/2}} \tag{41}$$

where b and c are positive constants. Since (40) is valid only if Λ_{eff} is negative, the above profiles apply only to an AdS_3 background. An important point is that the profile of

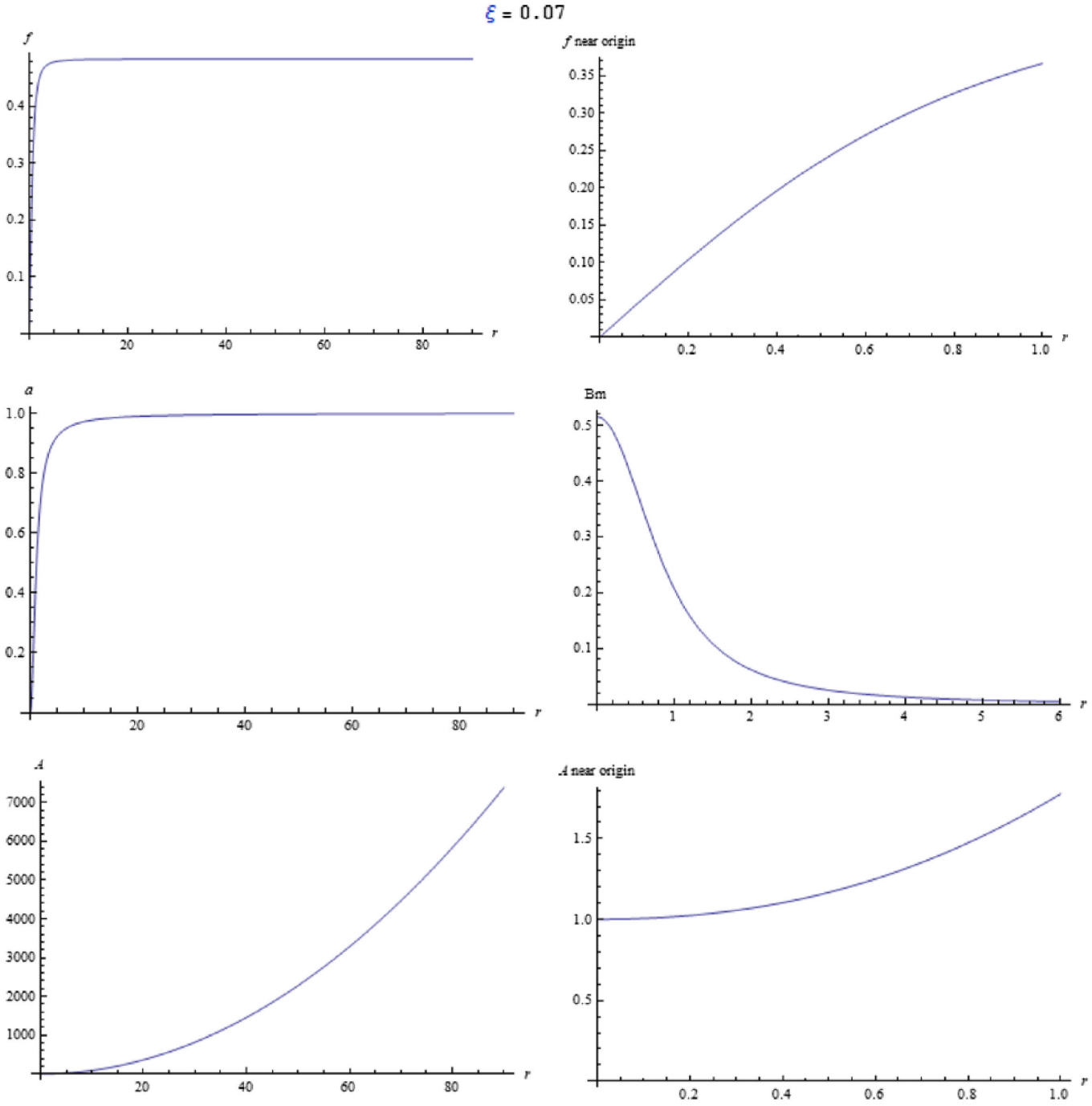

FIG. 9. Case $\xi = 0.07$. The regular plot of f vs r has a computational boundary of $R = 90$. The plot of f near the origin shows that f is now quite far from its plateau value. It now requires a larger radial distance before it plateaus to its VEV. There is no longer any dip in the metric function A: The numerical values show that $A(r)$ increases monotonically. The magnetic field B_m, just like f, extends out much further than previously.

a vortex which requires the gauge field a to plateau at n and f to plateau at $v_{\rm eff}$ is not supported by a positive $\Lambda_{\rm eff}$. It is supported by a negative $\Lambda_{\rm eff}$ and, as we will see, also by a zero $\Lambda_{\rm eff}$. The vortex therefore exists only in an AdS_3 or Minkowski background.

When $\Lambda_{\rm eff} = 0$, asymptotically we have $A(r) = D$ where D is positive [since a nonsingular profile requires that $A(r) > 0$]. We also have $v_{\rm eff} = v$. The differential equations governing the perturbations ϵ and β are then

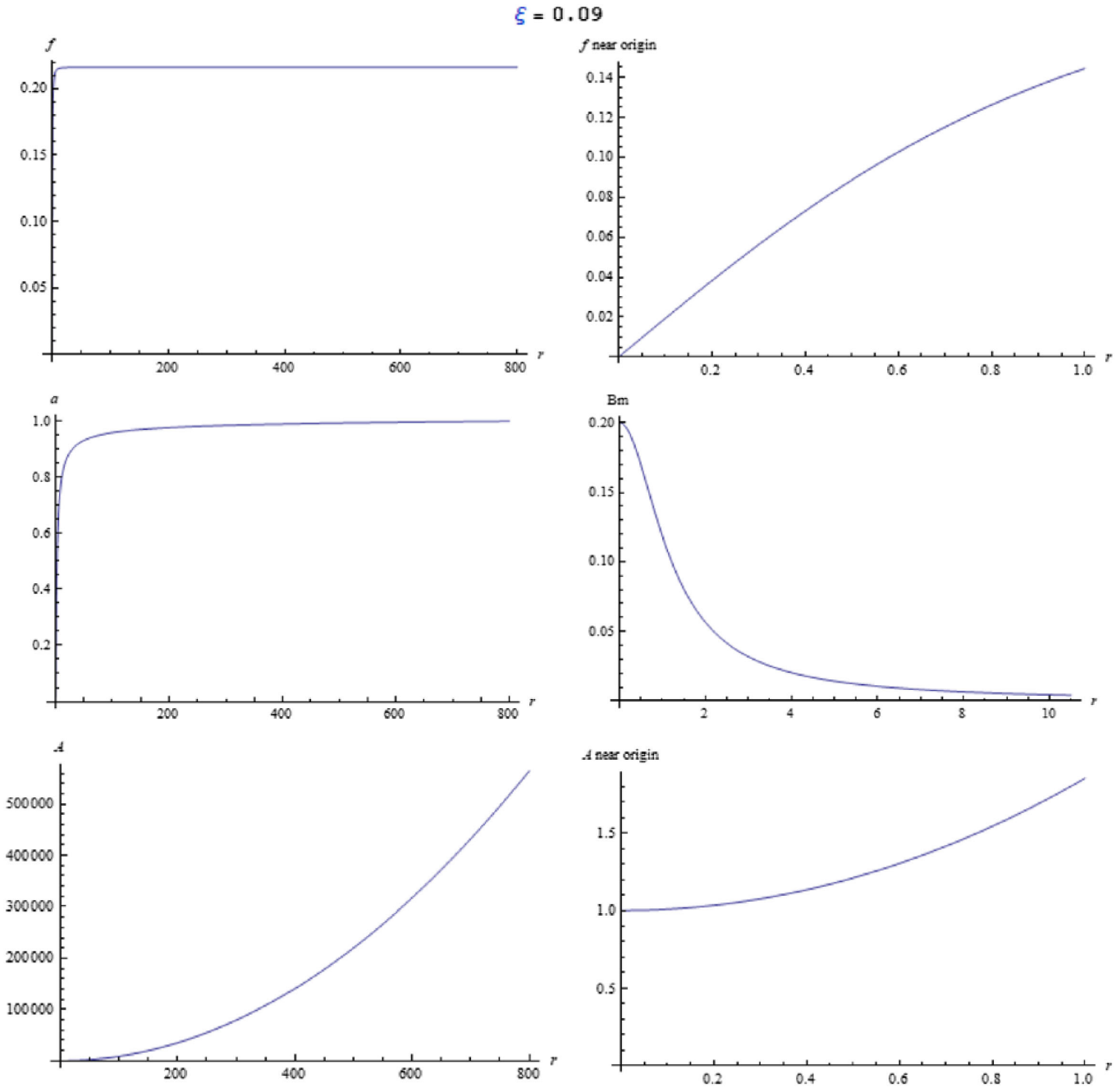

FIG. 10. Case $\xi = 0.09$. This is the second largest ξ in our sample, and we are now getting quite close to the critical coupling $\xi_c \approx 0.0952$ where the derivative of the VEV with respect to ξ diverges. The change from $\xi = 0.07$ to $\xi = 0.09$ is therefore large. The regular plot of f vs r has a significantly larger computational boundary of $R = 800$. The plot of f near the origin shows that f is very far from its plateau value. It now requires a very large radial distance before it plateaus to its VEV. Again, there is no longer any dip in the metric function A, and it increases monotonically. The magnetic field B_m, just like f, extends out again much further than previously.

$$e^2 r v^2 \epsilon(r) + D(\epsilon'(r) - r\epsilon''(r)) = 0, \tag{42}$$

$$2rv^2\lambda(\alpha + v^2\xi)\beta(r) - D(\alpha + v^2\xi(1 + 8\xi))(\beta'(r) + r\beta''(r)) = 0 \tag{43}$$

with solutions

$$\epsilon(r) = be^{\frac{-evr}{\sqrt{D}}}\sqrt{r}, \tag{44}$$

$$\beta(r) = ce^{-vr\left(\frac{2\lambda\alpha_{\text{eff}}}{D(\alpha_{\text{eff}}+8v^2\xi^2)}\right)^{1/2}} \frac{1}{\sqrt{r}} \tag{45}$$

where b and c are positive constants. The above result is for a Minkowski background ($\Lambda_{\text{eff}} = 0$) but where

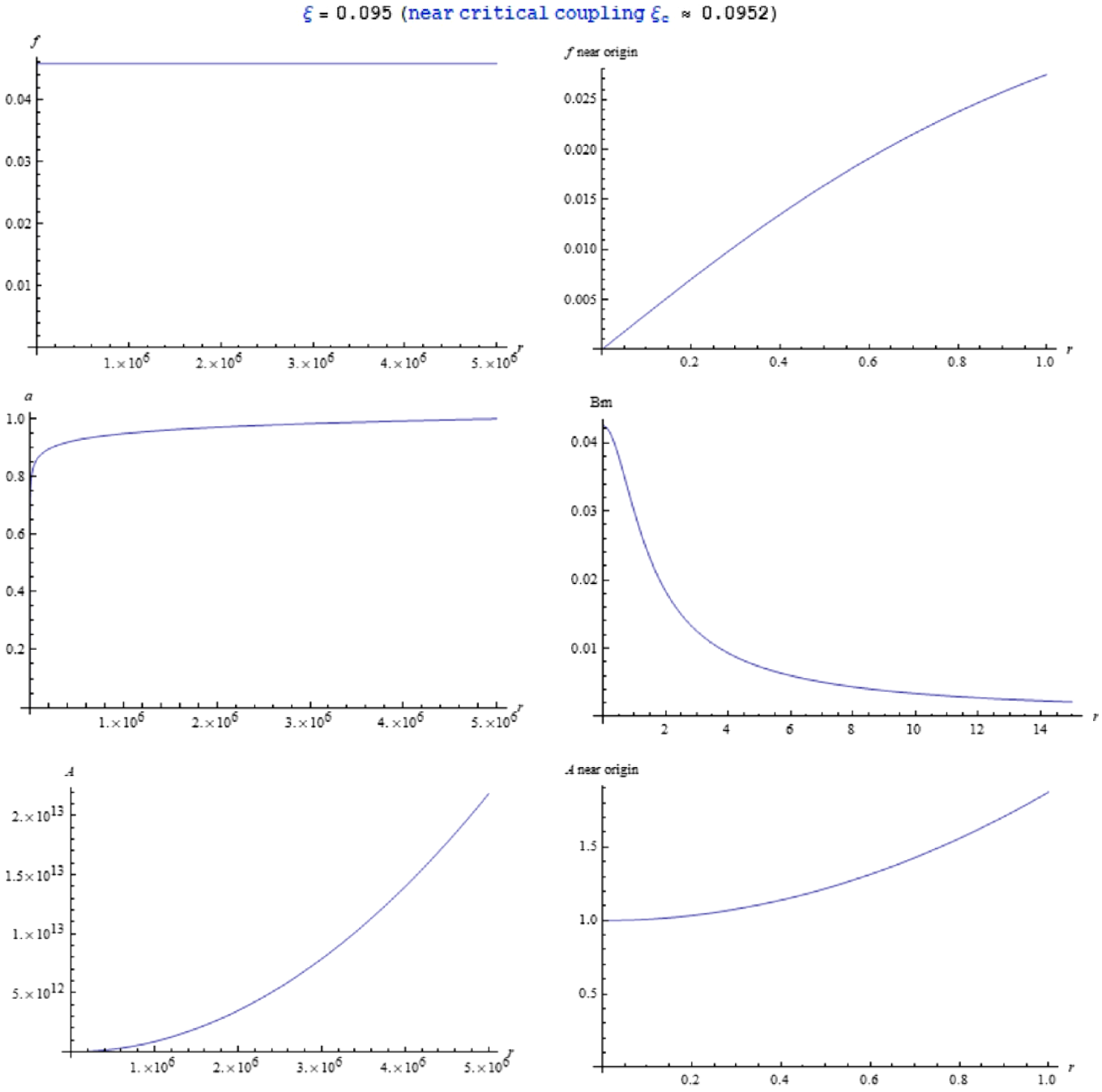

FIG. 11. Case $\xi = 0.095$. This is the largest ξ in our sample, and it is very close to the critical coupling $\xi_c \approx 0.0952$. Since we are near the critical point, the change from $\xi = 0.09$ to $\xi = 0.095$ is very large. The plot of f near the origin shows that f is again very far from its plateau value; this is why the regular plot of f vs r requires an extremely large computational boundary of $R = 5 \times 10^6$. This is the radius required for f to reach its VEV to the same level of accuracy as the other cases. The "extension" of f (a measure of the radius required to reach the VEV) therefore increases enormously as ξ approaches the critical coupling ξ_c, and this is analogous to the divergence of the coherence length in GL mean-field theory as one approaches the critical temperature T_c.

TABLE I. We present data for ξ ranging from -0.14 to 0.095 (near the critical coupling $\xi_c = 2/21 \approx 0.0952$). The theoretically predicted values of the VEV $v_{\rm eff}$ and cosmological constant $\Lambda_{\rm eff}$ calculated using (7) and (8), respectively, match the numerical values to within three or four decimal places. The peak value of the magnetic field occurs at the origin and also decreases monotonically as ξ increases. The magnetic flux obtained by integrating numerically over the magnetic field profile remains constant despite the different profiles, and its numerical value matches the theoretically expected value of $\Phi = 2\pi n/e = 2.0944$ to within three or four decimal places. This provides a very strong check on our numerical simulation. The ADM mass increases from $\xi = 0.095$ to $\xi = -0.12$, but this trend does not extend all the way to $\xi = -0.14$; this is due to a significant negative gravitational binding energy in the case of $\xi = -0.14$ (see body of the article for more details).

Coupling ξ	$V_{\rm eff}$ (theory)	$V_{\rm eff}$ (numeric)	$\Lambda_{\rm eff}$ (theory)	$\Lambda_{\rm eff}$ (numeric)	Mass (ADM)	Peak magnetic field	Magnetic flux (numeric)
−0.14	1.6475	1.6475	−1.0204	−1.0204	4.17	12.280	2.0944
−0.12	1.5766	1.5763	−1.0318	−1.0316	4.31	5.443	2.0944
−0.10	1.4990	1.4983	−1.0391	−1.0388	4.25	4.127	2.0943
−0.05	1.2733	1.2732	−1.0357	−1.0358	3.53	2.439	2.0946
0.0	1.000	1.0000	−1.000	−1.000	2.59	1.493	2.0943
0.05	0.6604	0.6604	−0.9398	−0.9398	1.50	0.783	2.0944
0.07	0.4839	0.4839	−0.9117	−0.9117	1.05	0.515	2.0945
0.09	0.2161	0.2161	−0.8827	−0.8827	0.45	0.200	2.0945
0.095	0.04584	0.04584	−0.8753	−0.8753	0.063	0.0425	2.0944

Einstein gravity and a nonminimal coupling term act on the vortex. The exponential falloff expressions (44) and (45) are similar to those found in fixed Minkowski spacetime [16], and we recover them if we set $\xi = 0$ and $D = 1$.

B. Plot of vortex profiles and magnetic field in AdS_3 for different ξ

The parameters that appear in the Lagrangian density (17) for the vortex are λ, e, n, v, α, Λ, and ξ. The goal here is to determine how the vortex changes with the coupling ξ and to observe what happens as we approach the critical coupling ξ_c. How the vortex changes with the other parameters such as Λ, n, and v has been studied elsewhere [3]. We therefore run numerical simulations for different values of ξ with the other parameters held fixed; we set $\lambda = 1$, $e = 3$, $n = 1$, $v = 1$, $\alpha = 1$, and $\Lambda = -1$. We work in natural units where $\hbar = c = 1$. Though our parameters and quantities such as the radius, mass, and magnetic field are quoted as numbers, they should be thought of as having a unit attached to them (except for the winding number n which is a pure number).[3] As we have seen, a negative Λ automatically ensures that the asymptotic cosmological constant $\Lambda_{\rm eff}$ will be negative. Our solutions in this section will therefore correspond to an AdS_3 background. Note that though v and Λ are held fixed, the VEV $v_{\rm eff}$ and the cosmological constant $\Lambda_{\rm eff}$ will change with ξ.

Recall that a critical coupling ξ_c exists only if $v^4\lambda + 8\alpha\Lambda$ is negative. With the above values for the parameters, this latter quantity is negative (equal to -7) and therefore a critical coupling exists. It is given by (11) and, substituting the values of our parameters, is equal to $\xi_c = 2/21 \approx 0.0952$ (the same value that appears in our plot of the VEV vs ξ in Fig. 1). This implies that for $\xi \geq 2/21$ the VEV is zero and there is no vortex. We therefore obtain vortices for $\xi < 2/21$.

We consider nine values of the coupling ξ that range from -0.14 to 0.095 (close to the upper bound ξ_c) which includes the case $\xi = 0$. We present Figs. 3–11, one for each value of the couplings in order of increasing ξ. Each figure contains plots of the scalar field $f(r)$, the gauge field $a(r)$, the metric function $A(r)$, and the magnetic field $B_m(r)$. We also made separate plots of f and A that focus on the core region near the origin where the fields undergo significant change. Therefore, there are six plots associated with each value of ξ. We also present some numerical results in table format. In Table I, we present the following data for each value of ξ: the theoretically expected and numerically obtained values of the VEV $v_{\rm eff}$ and cosmological constant $\Lambda_{\rm eff}$, the (ADM) mass of the vortex, the peak value of the magnetic field at the origin, and the numerically integrated magnetic flux.

In Table I, the formula (7) for the VEV $v_{\rm eff}$ matches almost exactly (to within three or four decimal places) the value where f plateaus numerically. Similarly, our formula (8) for the cosmological constant $\Lambda_{\rm eff}$ matches almost exactly (again to within three or four decimal places) the numerical value of the asymptotic cosmological constant.

[3] In AdS_3 the appropriate length scale is the AdS length ℓ. From (27), the quantity $-\Lambda_{\rm eff} r^2$ must be dimensionless. We quote $\Lambda_{\rm eff}$ as a pure negative number, but one should think of a unit y attached to it so that $\Lambda_{\rm eff} \times y = -1/\ell^2$. Therefore, the unit attached to the radius r is $y^{-1/2}$ which in terms of the AdS length is $(-\Lambda_{\rm eff})^{1/2}\ell$. Note that the equation for $\epsilon(r)$ in (41) implies that $e v_{\rm eff}/(-\Lambda_{\rm eff})^{1/2}$ is dimensionless. The quantity λ/e^2 is also dimensionless. The mass is proportional to $\alpha_{\rm eff} = \alpha + v_{\rm eff}^2\xi$; therefore, the mass is expressed in units of the VEV squared, which is $y^{1/2}$, and this can be expressed in terms of the inverse of the AdS length. The magnetic field is given by $B_m = \frac{\sqrt{A}a'}{er}$, and since $A(r)$ and $a(r)$ are dimensionless, it has units of $y^{3/4}$ which can be expressed in terms of the inverse of the AdS length to the power of $3/2$.

This provides strong confirmation of both our analytical formulas and the numerical simulation. In Figs. 3–11, the magnetic field B_m always peaks at the origin and then falls off with radius towards zero. As ξ increases and approaches closer to the critical coupling, the value of the peak magnetic field decreases (see plot in Fig. 13), but the magnetic field extends further out since it falls off to zero more slowly. As a consequence, the magnetic flux obtained numerically by integrating over the magnetic field profile remains constant as ξ changes (see Table I) and matches exactly (to within three or four decimal places) the expected theoretical value of $\Phi = 2\pi n/e = 2\pi/3 = 2.0944$ (where we substituted $n = 1$ and $e = 3$). That this numerically integrated magnetic flux remains constant across different magnetic field profiles provides another strong check on our numerical simulation.

In Table I, the VEV monotonically decreases from a value of 1.6475 at $\xi = -0.14$ to a value of 0.04584 at $\xi = 0.095$. We plot the nine data points in Fig. 12, and they trace out a curve similar to the plot in Fig. 1 of the VEV vs ξ obtained theoretically and hence also similar to the plot in Fig. 2 of the order parameter vs temperature in GL mean-field theory. We now verify numerically that the data points in our sample that are close to the critical coupling $\xi_c = 2/21$ follow the power law with critical exponent $1/2$ that we previously derived for ξ near ξ_c, i.e., $v_{\text{eff}} = k(\xi_c - \xi)^{1/2}$ where $k = \frac{v}{\sqrt{\xi_c + (2v^2\xi_c^2)/\alpha}}$ [see (13)]. For the values of our parameters, we obtain $k = 2.96985$. For $\xi = 0.095$, which is the closest data point to ξ_c in our sample, we obtain $k(\xi_c - \xi)^{1/2} = 0.04583$, which matches almost exactly our numerical result of 0.04584 for the VEV quoted in Table I. Another data point we can consider is $\xi = 0.09$ as it is not that far off from the critical coupling. This yields $k(\xi_c - \xi)^{1/2} = 0.2149$, which still matches quite closely our numerical result of 0.2161. This constitutes a quantitative confirmation that the nonminimally coupled vortex in AdS_3 undergoes critical phenomena with exponent $1/2$ at the critical coupling ξ_c.

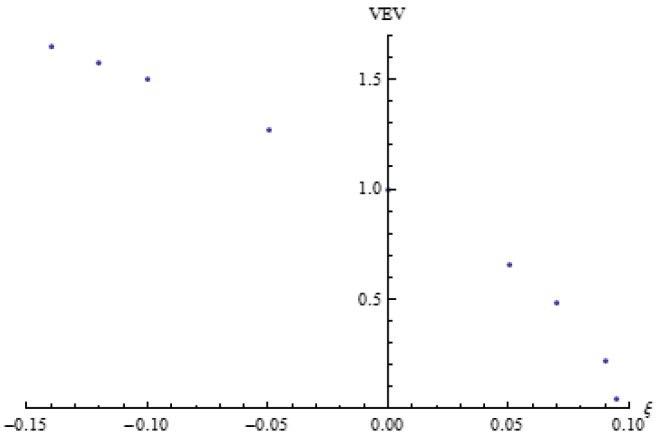

FIG. 12. Plot of the numerical value of the VEV vs ξ. The data points trace out a curve similar to the plot in Fig. 1 of the VEV vs ξ that was obtained theoretically, and similar to the curve in Fig. 2 of the order parameter vs temperature in GL mean-field theory. The VEV decreases monotonically, and its slope gets steeper (more negative) as ξ increases towards the critical coupling. The data points near ξ_c obey the power law $v_{\text{eff}} \propto (\xi_c - \xi)^{1/2}$ (see body of the article above for exact comparison); this confirms that our system undergoes critical phenomena with a critical exponent of $1/2$.

We mentioned above that the magnetic field extends further out as ξ increases towards the critical coupling ξ_c. The same thing happens with the scalar field f. For cases $\xi = -0.14$, $\xi = -0.12$, and $\xi = -0.10$, f can be seen to roughly plateau already near the origin (see plots of f near the origin in Figs. 3–5). At higher ξ, f has not plateaued yet near the origin (see plots of f near the origin in Figs. 6–11). This implies that it must extend further out to reach its VEV. In particular, as ξ approaches near the critical coupling ξ_c, the regular plot of f vs r has to be extended to drastically larger radii to accommodate the fact that f plateaus so much more slowly. We discuss the extension of the scalar field (and of the magnetic field) in more detail in the next subsection.

If the local matter density in the core region of the vortex is high enough, it causes a noticeable dip of the metric function $A(r)$ near the origin: The metric starts at $A = 1$ at the origin $r = 0$, dips below unity in the core region, and reaches a minimum that is above zero before increasing to reach its asymptotic r^2 dependence. The dip can be seen in the plot of A near the origin, and the asymptotic r^2 dependence is more evident in the regular plot of A vs r. The plots of the metric function $A(r)$ near the origin in Figs. 3–11 reveal that the dip monotonically decreases as ξ increases and is most pronounced at $\xi = -0.14$. This implies that the local matter density in the core region is

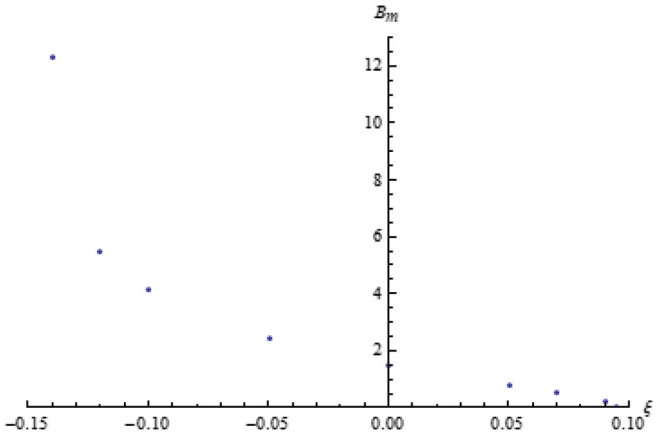

FIG. 13. Plot of peak magnetic field vs ξ. Like the VEV, it decreases monotonically as ξ increases, but in sharp contrast to the VEV, its slope gets flatter (less negative) as ξ increases towards the critical coupling. Therefore, the peak magnetic field does not act like an order parameter.

greatest for $\xi = -0.14$. Though A in this case dips the closest to zero (i.e., its minimum is the smallest), it does not cross zero. If A crosses zero, this would signal black hole formation and a singularity. However, our nonsingular initial conditions prevent one from constructing vortices beyond a local matter density where gravity becomes so strong that the scalar field is no longer able to reach its asymptotic plateau value. The fact that f is fixed to be zero at the origin prevents one from constructing vortex solutions when gravity's effect gets too strong. This places a lower bound on ξ; for the values of our parameters, we are not able to construct nonsingular vortices roughly below $\xi = -0.14$. This lower bound is reached way before the lower bound set by the condition $\alpha_{\rm eff} = \alpha + v_{\rm eff}^2 \xi > 0$. With $v_{\rm eff}$ given by (7) and using the values of our parameters, one can readily check that this would have occurred at the much lower value of $\xi = -0.26$.

In Table I, one can see that the ADM mass is highest at $\xi = -0.12$ and decreases afterwards as ξ increases towards $\xi = 0.095$. There is one case that does not follow this trend in masses. The ADM mass at $\xi = -0.14$ is actually lower than the mass at $\xi = -0.12$ (the data points of mass vs ξ are plotted in Fig. 14, and the curve nicely illustrates the trend in masses). The case $\xi = -0.14$ has the highest VEV, which would seem to imply that it should have the highest mass (vortices with higher VEVs will usually have more mass in fixed Minkowski spacetime [16]). Why then is the mass lower for $\xi = -0.14$ than for $\xi = -0.12$? This is due to the fact that the ADM mass receives contributions not only from matter but also from the negative binding energy of the gravitational field (see Sec. 3.9 on "Thin-shell collapse" in [17] for a clear illustration of this). The metric field $A(r)$ near the origin for $\xi = -0.14$ (Fig. 3) has a more pronounced dip than for $\xi = -0.12$ (Fig. 4). So the negative gravitational binding energy is significant enough in $\xi = -0.14$ to yield a lower ADM mass than in $\xi = -0.12$.

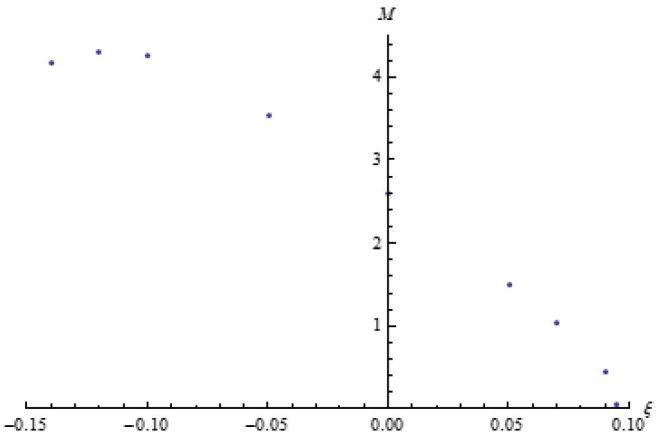

FIG. 14. Plot of mass M vs ξ. Near the critical coupling, this plot looks similar to the one for the VEV; in particular, its slope gets steeper (more negative) as ξ increases towards the critical coupling. The mass increases as ξ decreases, but unlike the VEV, this trend stops when we get to the most negative point, $\xi = -0.14$, where the mass is less than that for $\xi = -0.12$ due to gravity's effect (see discussion in body of the article).

1. Extension of scalar field and magnetic field and divergence at critical coupling ξ_c

We have already mentioned that as ξ increases towards the critical coupling, the scalar field and magnetic field extend further out. In the case of the scalar field, this means it rises more slowly and plateaus at its VEV over a longer radius. For the magnetic field, this means that starting from its peak at the origin, it decreases towards zero in a slower fashion, again over a longer radius. In short, the core region of the vortex occurs over a longer spatial range as ξ gets larger.

To make this more quantitative, we define the extension r_f of the scalar field to be the radius where it reaches 99.9%

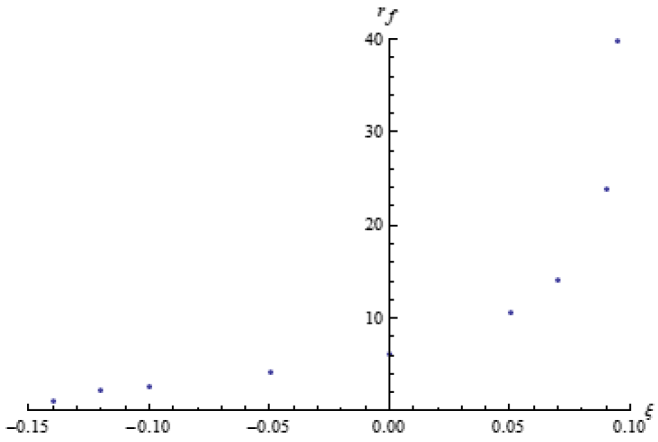

FIG. 15. Extension of the scalar field $f(r)$ as a function of ξ. Note the rapid increase in the extension as one approaches the critical coupling $\xi_c \approx 0.0952$. The extension is expected to diverge at the exact value of $\xi_c = 2/21$.

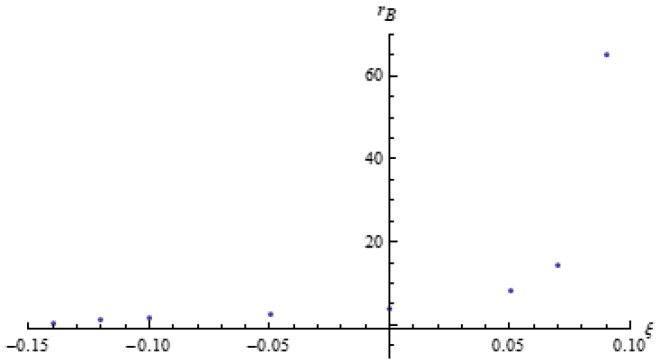

FIG. 16. Extension of the magnetic field $B_m(r)$ as a function of ξ. Here there is also a rapid increase in the extension as one approaches the critical coupling $\xi_c \approx 0.0952$. The extension is expected to diverge at the exact value of $\xi_c = 2/21$.

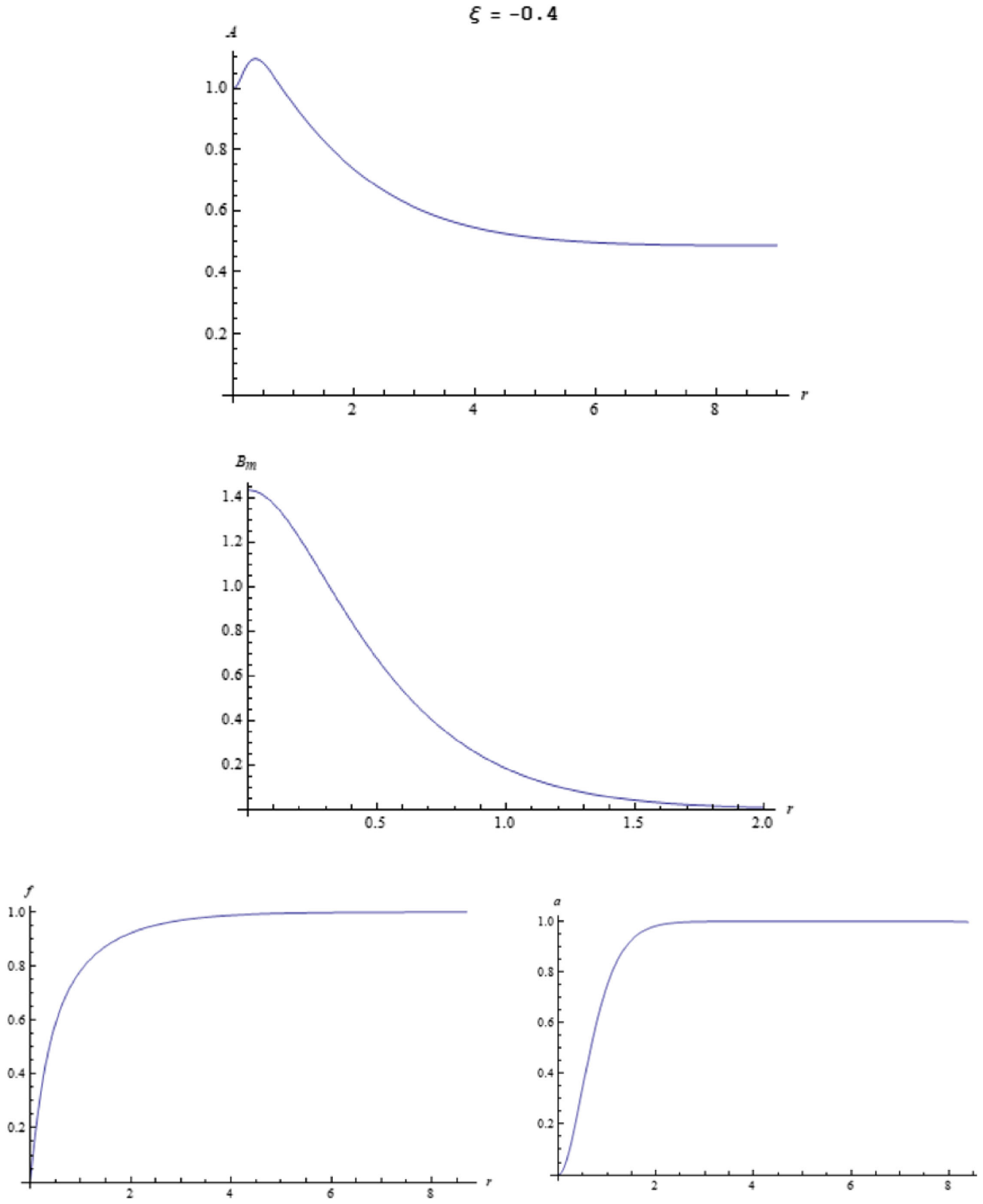

FIG. 17. Flat case $\xi = -0.4$. We plot the metric A, the magnetic field B_m, the scalar field f, and the gauge field a. Since the VEV of the scalar field is always unity, it plateaus at unity regardless of the value of ξ. The gauge field a always plateaus at unity also since $n = 1$ for all ξ. We therefore show the scalar and gauge field profiles here but not in subsequent figures since they are roughly similar. The metric profile plateaus at $D = 0.488$ which yields a deficit angle of 1.894 rad, the largest deficit angle in our sample but not the one with the highest mass (see Table II). The magnetic field peaks at 1.43, which is the highest peak in our sample. This implies that it extends the least (falls off fastest) since the magnetic flux remains constant at $\Phi = 2\pi n/e = 2.0944$ to within three or four decimal places.

of its VEV and define the extension r_B of the magnetic field to be the radius where it has fallen to 0.1% of its peak value (i.e., decreased by 99.9% from its peak at the origin). We plot in Fig. 15 the scalar field extension r_f vs ξ and in Fig. 16 the magnetic field extension r_B vs ξ. In both cases, there is a very rapid increase in the extension when ξ is near the critical coupling ξ_c. We see that the extension actually diverges at the exact value of $\xi = \xi_c = 2/21$. This is reminiscent of the divergence of the coherence length in GL mean-field theory at the critical temperature T_c.

We now show analytically that $f(r)$ approaches the VEV in the slowest fashion possible in the limit when ξ approaches ξ_c. If we let $f(r) = v_{\rm eff} - \beta(r)$ asymptotically, we know that $\beta(r)$ is given by (41), which we rewrite for convenience below:

$$\beta(r) = cr^{-1-\left[\frac{-\alpha_{\rm eff}\Lambda_{\rm eff}+2\alpha_{\rm eff}v_{\rm eff}^2\lambda-64v_{\rm eff}^2\Lambda_{\rm eff}\xi^2}{-\alpha_{\rm eff}\Lambda_{\rm eff}-16v_{\rm eff}^2\Lambda_{\rm eff}\xi^2}\right]^{1/2}} = cr^{-1-P^{1/2}} \tag{46}$$

where P is the quantity in square brackets. Since $\alpha_{\rm eff} > 0$ and $\Lambda_{\rm eff} < 0$, all the terms in the numerator and denominator in the square brackets are positive. It should be clear that $P \geq 1$. We have that β approaches zero asymptotically as $1/r^{1+P^{1/2}}$. When $\xi \to \xi_c$, we have that $v_{\rm eff} \to 0$ and $P \to 1$. Therefore, as $\xi \to \xi_c$, β decreases as $1/r^2$ asymptotically, which is the slowest falloff it can have, translating to the slowest approach that f can have towards its VEV.

Now r_f is the extension, defined as the radius where $f = 0.999v_{\rm eff}$ so that $r_f^{1+P^{1/2}}$ is proportional to $1/(0.001v_{\rm eff})$. This diverges as $\xi \to \xi_c$ since $v_{\rm eff} \to 0$. It is therefore expected that the extension r_f diverges at the critical coupling ξ_c in accordance with the trend in Fig. 15.

Asymptotically we have that $a(r) = n - \epsilon(r)$ where ϵ is given by (40). The magnetic field is given by $B_m = \sqrt{A(r)}a'(r)/(er)$. Asymptotically, $A(r) \to -\Lambda_{\rm eff}r^2$ and $a'(r) \to -\epsilon'(r)$ so that B_m falls off asymptotically as $r^{-\frac{ev_{\rm eff}}{(-\Lambda_{\rm eff})^{1/2}}-1}$. As $\xi \to \xi_c$, we have that $v_{\rm eff} \to 0$, so B_m falls off as $1/r$, which is the slowest falloff possible. The extension r_B is therefore proportional to the inverse of the peak magnetic field as $\xi \to \xi_c$. Our numerical results

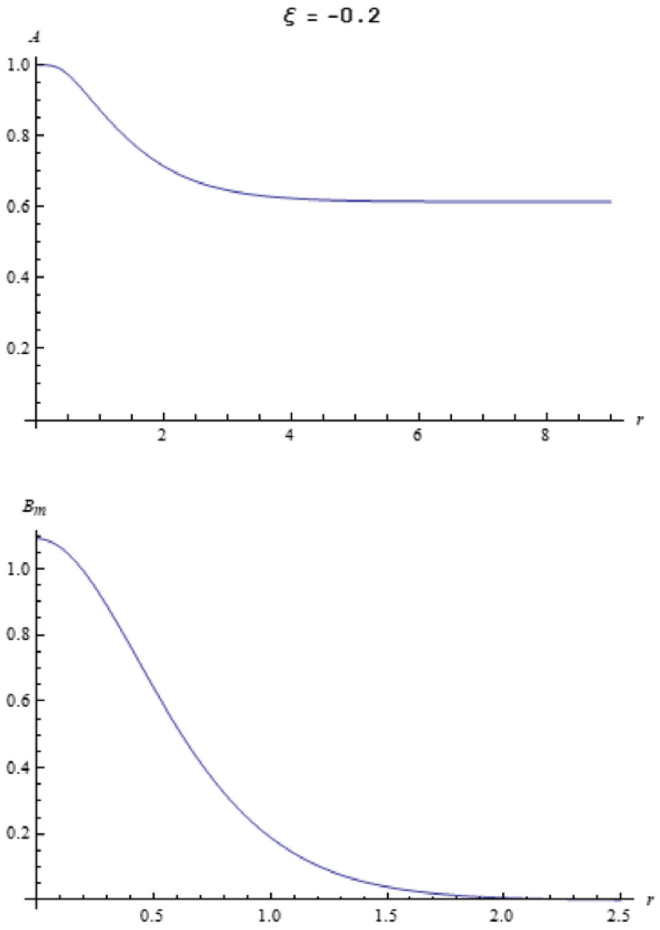

FIG. 18. Flat case $\xi = -0.2$. The metric A plateaus at $D = 0.615$ yielding a deficit angle 1.356 rad, the second largest deficit angle in our sample. The magnetic field peaks at 1.092, the second largest peak in our sample.

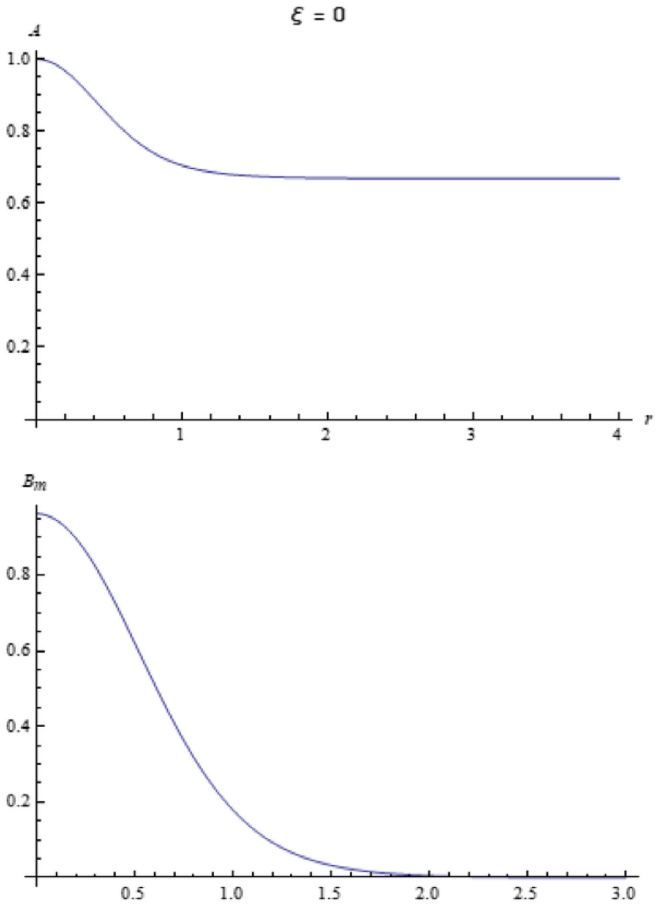

FIG. 19. Flat case $\xi = 0$. The nonminimal coupling is turned off here. The metric A plateaus at $D = 0.668$ yielding a deficit angle of 1.148. The magnetic field peaks at 0.962 and is less than the previous case.

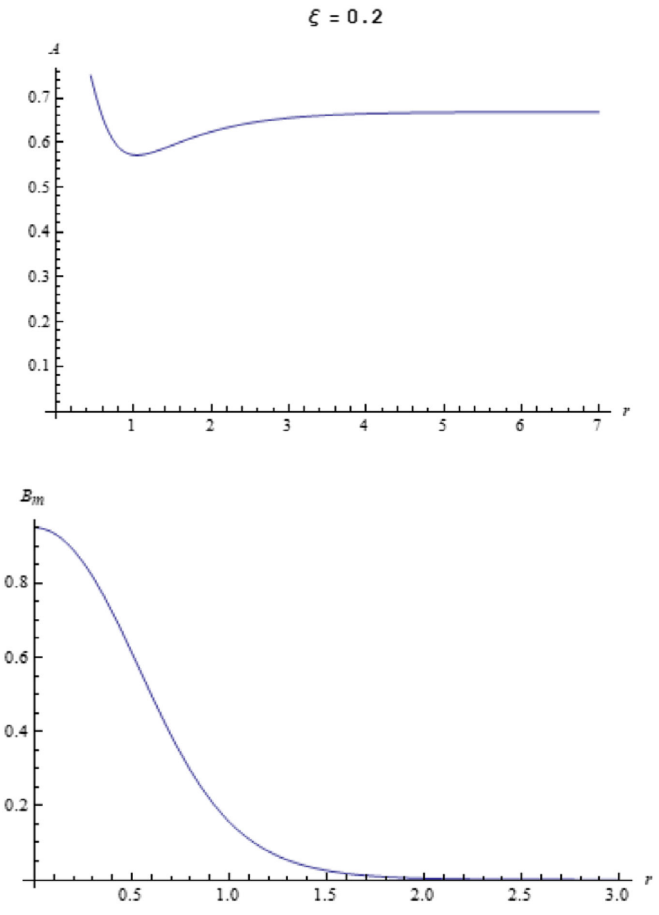

FIG. 20. Flat case $\xi = 0.2$. The metric A plateaus at $D = 0.668$, the same value as the previous case. It therefore also has a deficit angle of 1.148. It has a peak magnetic field of 0.950 which is less than the previous case. So far, there has been a trend: The peak of the magnetic field has monotonically decreased, and the deficit angle has decreased or remained the same.

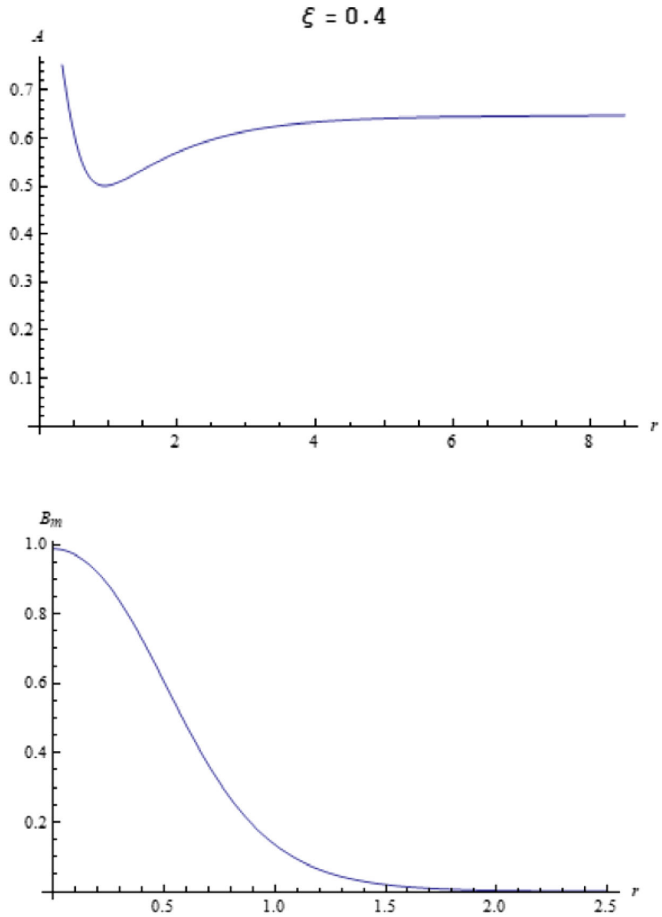

FIG. 21. Flat case $\xi = 0.4$. This case departs from the above decreasing trend. The metric plateaus at $D = 0.648$ yielding a deficit angle of 1.225 rad and a peak magnetic field of 0.987: Both are greater than in the previous two cases.

show that the peak value of the magnetic field at the origin keeps decreasing (towards zero) as $\xi \to \xi_c$, so the extension r_B tends to infinity. This agrees with the fact that the magnetic flux can remain constant as the peak magnetic field at the origin decreases to zero only if the magnetic field has an infinite extension.

C. Plot of vortex profiles and magnetic field in asymptotically Minkowski spacetime

We now consider the role the coupling ξ plays for the case of asymptotically Minkowski spacetime. This corresponds to $\Lambda = 0$ which as we have seen, implies $\Lambda_{\text{eff}} = 0$. As previously mentioned, there is no critical coupling for asymptotically Minkowski spacetime. The VEV is expected to remain constant at $v_{\text{eff}} = v = 1$, and the cosmological constant is expected to remain at $\Lambda_{\text{eff}} = 0$; i.e., the VEVs v_{eff} and Λ_{eff} have no dependence on ξ in contrast to the AdS_3 case. We run numerical simulations for different values of ξ with the same set of parameters as before: $\lambda = 1$, $e = 3$, $n = 1$, $v = 1$, and $\alpha = 1$. The only difference is that $\Lambda = 0$ now (instead of $\Lambda = -1$ in the AdS_3 case). We work again in natural units. As before, the parameters and quantities like the radius, mass, and magnetic field are quoted as numbers, but one should think of a unit attached to them.[4]

We made plots for five different cases: $\xi = \{-0.4, -0.2, 0.0, 0.2, 0.4\}$ corresponding to Figs. 17–21 respectively. The plots of the scalar field f and the gauge field a all plateau at unity regardless of ξ. We also plot the magnetic field whose profile depends on ξ. The most

[4]In Minkowski spacetime, the appropriate length scale is set by the VEV v. In particular, evr is dimensionless, where r is the radius. Though e and v are quoted as numbers, one should think of ev as having a unit x of dimension $[\mathrm{L}]^{-1}$ attached to it. It follows then that the radius r has units of x^{-1} which has the correct dimensions of [L]. The mass is proportional to the VEV squared and is therefore expressed in units of x which has the correct dimension of $[\mathrm{L}]^{-1}$. The magnetic field $B_m = \frac{\sqrt{A}a'}{er}$ is expressed in units of $x^{3/2}$ which has the correct dimensions of $[\mathrm{L}]^{-3/2}$. As before, λ/e^2 is dimensionless.

TABLE II. The most important point about this table is that the deficit angle is not proportional to the mass. Compare the first and last rows. At $\xi = -0.4$ one has the largest deficit angle of 1.894 rad with a mass of 2.273 whereas at $\xi = +0.4$ the mass is significantly higher at 3.430 and yet it has a much smaller deficit angle of 1.225 rad. With the nonminimal coupling term present, the ratio of mass to deficit angle is not constant but depends on ξ (see body of the article).

Coupling ξ	D (plateau value of metric A)	δ Deficit angle (rad)	Mass	Peak value of magnetic field
−0.4	0.488	1.894	2.273	1.433
−0.02	0.615	1.356	2.170	1.092
0.0	0.668	1.148	2.296	0.962
0.2	0.668	1.148	2.755	0.950
0.4	0.648	1.225	3.430	0.987

important plot by far is the one for the metric A which plateaus asymptotically to a constant value (which we previously labeled D). The profile of the metric here (starting at unity at the origin and then plateauing to $0 < D < 1$) is in stark contrast to the AdS_3 case where the metric had an r^2 dependence asymptotically. The constant D can only be obtained numerically (by running the simulation), and it changes with ξ. Since the deficit angle depends on D via (34), the deficit angle depends on ξ. We also calculate the mass $M_{\rm flat}$ of the vortex via (33). The constant D, the deficit angle δ, the mass $M_{\rm flat}$ as well as the peak value of the magnetic field are presented in Table II. In $2+1$-dimensional general relativity in asymptotically Minkowski spacetime, there is the classic result of Deser *et al.* [7] that a point mass produces a deficit angle proportional to the mass. The ratio of mass to deficit angle is equal to $2\alpha = 1/(8\pi G)$ and is a constant since Newton's constant G does not change as the mass changes. In contrast, for the vortex with nonminimal coupling, the ratio of mass to deficit angle is not constant but depends on ξ: It is equal to $2\alpha_{\rm eff} = 2(\alpha + v^2\xi) = 2(1+\xi)$ where we substituted the values $\alpha = 1$ and $v = 1$ for our parameters. A striking consequence is that it is possible for a larger mass to actually produce a smaller deficit angle compared to a smaller mass. For example, in Table II, the case at $\xi = -0.4$ has the largest deficit angle of 1.894 rad in our sample and has a mass of 2.273, whereas the case at $\xi = 0.4$ has a smaller deficit angle of 1.225 rad but the largest mass of 3.430 in our sample, which is roughly 1.5 times greater than our former case.

VIII. CONCLUSION

In this paper, we studied the effects of the nonminimal coupling term $\xi R|\phi|^2$ on a vortex under Einstein gravity in an AdS_3 and flat (conical) background. In the case of AdS_3, this led to the emergence of a critical coupling ξ_c where the VEV of the scalar field is zero for ξ at or above ξ_c but nonzero when ξ crosses below ξ_c. For the values of our parameters, ξ_c is equal to $2/21 \approx 0.0952$. We presented our numerical results in plots and tables for nine values of ξ. Our plot of the numerically obtained VEV versus ξ is in accordance with the theoretical expectation that the slope has a discontinuity and diverges at the critical coupling ξ_c. For ξ near ξ_c, we verified numerically that the VEV indeed behaved according to the power law $|\xi - \xi_c|^{1/2}$. These results confirmed the idea that the critical coupling ξ_c acts like the analog of the critical temperature T_c in GL mean-field theory. In that theory, the order parameter is zero at or above T_c and nonzero below T_c and behaves according to the power law $|T - T_c|^{1/2}$. The plot of the order parameter versus temperature T also shows a discontinuity and divergence in the slope near T_c. Numerical results of the "extension" of the scalar field (core region of the vortex) show that it increases monotonically as ξ increases, with a dramatic increase near ξ_c. We showed analytically that it is expected to diverge at the critical coupling, and this is analogous to the divergence of the coherence length in GL mean-field theory as one approaches the critical temperature.

In asymptotically flat (conical) spacetime, we considered five values of ξ and, remarkably, found that higher masses did not necessarily lead to a higher deficit angle as one might naively expect. The reason for this is that, when a nonminimal coupling term is present, the ratio of mass to deficit angle is no longer constant but depends on the coupling ξ. This can lead to cases where a higher mass has a smaller deficit angle than a smaller mass as our data clearly showed.

If ξ_c acts as the analog to T_c in GL mean-field theory, this naturally raises the question, "Is the nonminimally coupled vortex a thermodynamic system at nonzero temperature?". The answer is clearly no. The Nielsen-Olesen vortex without gravity constitutes a static classical field configuration which is at zero temperature and has zero entropy. The zero temperature agrees with the fact that the fields have no average kinetic energy, and the zero entropy is in accordance with the fact that we know everything about the field's configuration throughout spacetime; we are not ignorant of its configuration at any time, and no information is hidden from us. The zero entropy is of course consistent with the zero temperature. When gravity is included, this can change only if the vortex acquires an event horizon. However, our gravitating vortex solutions are nonsingular static solutions with no event horizon. The temperature and entropy are again zero, and as before, the metric field, as well as the scalar and gauge fields, are static throughout all of spacetime. In contrast, the BTZ black hole [8,9] has a nonzero temperature and entropy as it has an event horizon (for simplicity, assume no angular momentum or electric charge, only mass with a single horizon). Note that the BTZ spacetime has a timelike Killing vector outside the event horizon, but like the Schwarzschild black

hole in $3+1$ dimensions, it has no timelike Killing vector inside the event horizon [18]. This implies that there is no coordinate transformation that can put the metric in static form inside the event horizon, so an outside observer is ignorant of the metric configuration inside at any particular time. Simply put, information is hidden from us behind the event horizon [19]. Note that in contrast, our nonsingular gravitating static vortex has a timelike Killing vector throughout spacetime, and no information is hidden from us (see also [20–22] for a related discussion).

The vortex actually constitutes a classical solution in quantum field theory (QFT) [16]. The vortex cannot be obtained from perturbative QFT as it is a nonperturbative solution. It turns out that since the size of the vortex is much larger than its Compton wavelength, the classical nonperturbative solution constitutes a valid solution to the QFT (i.e., a very good first approximation) [16]. Perturbation theory can then be used to obtain one-loop quantum corrections to the vortex by quantizing about the classical configuration. In particular, quantum fluctuations of the scalar field will change the nature of the potential as there will now be logarithmic terms besides the usual terms [23,24]. The critical exponent of $1/2$ will therefore change as a consequence of these quantum corrections. So an interesting and pertinent problem to solve for the future is to determine the critical exponent of the nonminimally coupled vortex in an AdS_3 background after quantum corrections. This would be a considerably more complicated calculation than, say, the quantization about the $1+1$-dimensional kink in Minkowski spacetime [16] as we have one extra spatial dimension and a curved space background.

ACKNOWLEDGMENTS

A. E. acknowledges support from a discovery grant of the National Science and Engineering Research Council of Canada (NSERC).

APPENDIX A: DERIVATION OF THE VEV v_{eff} AND COSMOLOGICAL CONSTANT Λ_{eff}

In this appendix we derive the expressions for v_{eff} and Λ_{eff} given by Eqs. (7) and (8), respectively. We start by rewriting Eqs. (5) and (6) where v_{eff} and Λ_{eff} are expressed in terms of each other:

$$v_{\mathrm{eff}}^2 = v^2 + \frac{12\xi\Lambda_{\mathrm{eff}}}{\lambda}, \tag{A1}$$

$$\alpha(R-2\Lambda)+\xi R v_{\mathrm{eff}}^2 - \frac{\lambda}{4}(v_{\mathrm{eff}}^2 - v^2)^2 = (\alpha+\xi v_{\mathrm{eff}}^2)(R-2\Lambda_{\mathrm{eff}}). \tag{A2}$$

We first substitute the asymptotic value of the Ricci scalar, $R = 6\Lambda_{\mathrm{eff}}$, into (A2) which yields

$$\Lambda_{\mathrm{eff}} = \frac{\alpha\Lambda + \frac{\lambda}{8}(v_{\mathrm{eff}}^2 - v^2)^2}{\alpha + \xi v_{\mathrm{eff}}^2}. \tag{A3}$$

Substituting (A3) into (A1) yields a quadratic equation for v_{eff}^2:

$$\lambda\xi(v_{\mathrm{eff}}^2)^2 - 2\lambda(\alpha+2v^2\xi)v_{\mathrm{eff}}^2 + 2v^2\alpha\lambda + 3v^4\lambda\xi + 24\alpha\Lambda\xi = 0. \tag{A4}$$

This yields the following two possible solutions for v_{eff}^2 (which we label I and II):

$$\mathrm{I}: \quad 2v^2 + \frac{\alpha}{\xi} - \frac{\sqrt{\alpha^2 + 2v^2\alpha\xi + v^4\xi^2 - 24\alpha\Lambda\xi^2/\lambda}}{\xi}, \tag{A5}$$

$$\mathrm{II}: \quad 2v^2 + \frac{\alpha}{\xi} + \frac{\sqrt{\alpha^2 + 2v^2\alpha\xi + v^4\xi^2 - 24\alpha\Lambda\xi^2/\lambda}}{\xi}. \tag{A6}$$

However, only the first solution satisfies the requirement that v_{eff} is equal to v in the limit $\xi \to 0$. The second solution yields ∞ in that limit and must be disregarded. Taking the positive of the square root of the first solution yields the quoted result (7) for v_{eff}:

$$v_{\mathrm{eff}} = \left[2v^2 + \frac{\alpha}{\xi} - \frac{\sqrt{\alpha^2 + 2v^2\alpha\xi + v^4\xi^2 - 24\alpha\Lambda\xi^2/\lambda}}{\xi}\right]^{1/2}. \tag{A7}$$

Substituting the above solution (A7) into (A3) yields the quoted result (8) for Λ_{eff}:

$$\Lambda_{\mathrm{eff}} = \frac{\lambda}{12\xi^2}(\alpha + v^2\xi - \sqrt{\alpha^2 + v^4\xi^2 + 2v^2\alpha\xi - 24\alpha\Lambda\xi^2/\lambda}). \tag{A8}$$

APPENDIX B: FULL EQUATIONS OF MOTION

The three equations of motion quoted in the text are (23)–(25). Equation (25) contains the function $W(r) = B'/B$, and Eq. (24) contains W and its derivative W'. We can extract W from (19), and this yields

$$W = \frac{1}{4e^2rA(\alpha+\xi f^2+2r\xi ff')}(-e^2r^2(v^4\lambda+8\alpha\Lambda) - 2e^2(n^2 - r^2v^2\lambda - 2na + a^2)f^2 - e^2r^2\lambda f^4 - 16e^2r\xi Aff' + 2A(a'^2 + e^2r^2f'^2)). \tag{B1}$$

Substituting the above expression for W (as well as its derivative) back into (24) and (25) and keeping (23) the same yields three equations of motion that have no dependence on the function B. The three full equations are

$$e^2r^2\lambda f^4 + e^2r(rv^4\lambda + 8r\alpha\Lambda + 4\alpha A') + 2e^2f^2(n^2 - r^2v^2\lambda - 2na + a^2 + 2r\xi A') + 2A(a'^2 + e^2r^2(1+8\xi)f'^2) + 8e^2r\xi f(rA'f' + 2A(f' + rf'')) = 0, \tag{B2}$$

$$\begin{aligned}
&-2r^2\lambda f^3 - 2f(n^2 - r^2v^2\lambda - 2na + a^2 + 2r\xi A') + r(rA'f' + 2A(f' + rf'')) \\
&+ \frac{1}{8e^4A(\alpha + \xi f(f + 2rf'))^2}(\xi f(e^2r^2(v^4\lambda + 8\alpha\Lambda) - 2Aa'^2 \\
&+ e^2(2(n^2 - r^2v^2\lambda - 2na + a^2)f^2 + r^2\lambda f^4 + 16r\xi Aff' - 2r^2Af'^2))^2) \\
&+ \frac{r}{4e^4A(\alpha + \xi f(f + 2rf'))^2}\Bigg(2e^2\xi fA'(\alpha + \xi f(f + 2rf'))(e^2r^2(v^4\lambda + 8\alpha\Lambda) - 2Aa'^2 \\
&+ e^2(2(n^2 - r^2v^2\lambda - 2na + a^2)f^2 + r^2\lambda f^4 + 16r\xi Aff' - 2r^2Af'^2)) \\
&- e^2Af'(\alpha + \xi f(f + 2rf'))(e^2r^2(v^4\lambda + 8\alpha\Lambda) - 2Aa'^2 \\
&+ e^2(2(n^2 - r^2v^2\lambda - 2na + a^2)f^2 + r^2\lambda f^4 + 16r\xi Aff' - 2r^2Af'^2)) \\
&+ \frac{1}{r}\xi f\Bigg(-e^4(r^2(v^4\lambda + 8\alpha\Lambda) + 2(n^2 - r^2v^2\lambda - 2na + a^2)f^2 + r^2\lambda f^4) \\
&(r^2\lambda f^4 + r(rv^4\lambda + 8r\alpha\Lambda + 4\alpha A') + 2f^2(n^2 - r^2v^2\lambda - 2na + a^2 + 2r\xi A') + 8r^2\xi fA'f') \\
&- 4e^2A(-2e^2r^2\lambda\xi f^6 - r^2(v^4\lambda + 8\alpha\Lambda)(a'^2 + e^2(2\alpha + r^2(1-2\xi)f'^2)) \\
&- rf^4(4e^2\xi(-n + a)a' + r\lambda a'^2 + e^2r\lambda(2(\alpha - 2v^2\xi) + r^2(1+6\xi)f'^2)) \\
&- 2f^2(2e^2r\alpha(-n + a)a' + (n^2 - r^2v^2\lambda - 2na + a^2)a'^2 + e^2r^2(-2v^2\alpha\lambda + v^4\lambda\xi + 8\alpha\Lambda\xi \\
&+ (1+2\xi)(n^2 - r^2v^2\lambda - 2na + a^2)f'^2)) + 2e^2r^3\lambda\xi f^5(2f' + rf'') \\
&+ 2e^2rf(2(-n^2\alpha + r^2(v^2\alpha\lambda + 2v^4\lambda\xi + 16\alpha\Lambda\xi) + \alpha(2n - a)a)f' + r^3(v^4\lambda + 8\alpha\Lambda)\xi f'') \\
&+ 4e^2rf^3(-(-5n^2\xi + r^2\lambda(\alpha + 3v^2\xi) + 5\xi(2n - a)a + 2r\xi(-n + a)a')f' \\
&+ r\xi(n^2 - r^2v^2\lambda - 2na + a^2)f'')) - 4A^2\Big(a'^4 - 16e^4r\xi f(\alpha + \xi f^2)f' \\
&+ 4e^2ra'(\alpha + \xi f(f + 2rf'))a'' - 2e^2ra'^2(r(-1 + 2\xi)f'^2 + 2\xi f(6f' + rf'')) \\
&+ e^4r^2(-16r\xi ff'^3 + r^2(1 - 4\xi)f'^4 - 16\xi f(\alpha + \xi f^2)f'' \\
&+ 4r(\alpha + \xi f^2)f'f'' + 4f'^2(\alpha - 4\alpha\xi + \xi f(f + 20\xi f + r^2f'')))\Big)\Bigg)\Bigg) = 0,
\end{aligned} \tag{B3}$$

$$2e^2r(n-a)f^2 - 2Aa' + ra'A' + 2rAa'' + \frac{a'}{4e^2(\alpha + \xi f^2 + 2r\xi ff')}(-e^2r^2(v^4\lambda + 8\alpha\Lambda) - 2e^2(n^2 - r^2v^2\lambda - 2na + a^2)f^2 - e^2r^2\lambda f^4 - 16e^2r\xi Aff' + 2A(a'^2 + e^2r^2f'^2)) = 0. \tag{B4}$$

The above three equations are those we solve numerically.

[1] M. Cadoni, P. Pani, and M. Serra, Scalar hairs and exact vortex solutions in 3D AdS gravity, J. High Energy Phys. 01 (2010) 091.

[2] É. Dupuis, Y. Gobeil, B.-H. Lee, W. Lee, R. Mackenzie, M. B. Paranjape, U. A. Yajnik, and D.-h. Yeom, Tunneling decay of false vortices with gravitation, J. High Energy Phys. 11 (2017) 028.

[3] A. Edery, Non-singular vortices with positive mass in 2 + 1-dimensional Einstein gravity with AdS_3 and Minkowski background, J. High Energy Phys. 01 (2021) 166.

[4] J. Albert, The Abrikosov vortex in curved space, J. High Energy Phys. 09 (2021) 012.
[5] J. Zinn-Justin, *Phase Transitions and Renormalization Group* (Oxford University Press, Oxford, United Kingdom, 2007).
[6] J. F. Annett, *Superconductivity, Superfluids and Condensates* (Oxford University Press, Oxford, United Kingdom, 2004).
[7] S. Deser, R. Jackiw, and G. 't Hooft, Three-dimensional Einstein gravity: Dynamics of flat space, Ann. Phys. (N.Y.) **152**, 220 (1984).
[8] M. Bañados, C. Tetelboim, and J. Zanelli, Black Hole in Three-Dimensional Spacetime, Phys. Rev. Lett. **69**, 1849 (1992).
[9] M. Bañados, M. Henneaux, C. Tetelboim, and J. Zanelli, Geometry of the $2+1$ black hole, Phys. Rev. D **48**, 1506 (1993).
[10] E. Bergshoeff, O. Hohm, and P. Townsend, Massive Gravity in Three Dimensions, Phys. Rev. Lett. **102**, 201301 (2009).
[11] J. Oliva, D. Tempo, and R. Troncoso, Three dimensional black holes, gravitational solitons, kinks and wormholes for BHT massive gravity, J. High Energy Phys. 07 (2009) 011.
[12] P. Breitenlohner and D. Z. Freedman, Positive energy in anti-de Sitter backgrounds and gauged extended supergravity, Phys. Lett. **115B**, 197 (1982).
[13] S. R. Coleman and F. De Luccia, Gravitational effects on and of vacuum decay, Phys. Rev. D **21**, 3305 (1980).
[14] S. M. Carroll, *Spacetime and Geometry* (Pearson Education Inc., San Francisco, CA, 2004).
[15] C. Lygouras, "Critical behavior of the order parameter and specific heat in the second-order phase transition from Landau theory," May 4, 2020. Wikimedia Commons contributors, File:LandauTheoryTransitions.svg, Wikimedia Commons, the free media repository.
[16] E. J. Weinberg, *Classical Solutions in Quantum Field Theory* (Cambridge University Press, Cambridge, England, 2012).
[17] E. Poisson, *A Relativist's Toolkit* (Cambridge University Press, Cambridge, England, 2004).
[18] A. Edery and B. Constantineau, Extremal black holes, gravitational entropy and nonstationary metric fields, Classical Quantum Gravity **28**, 045003 (2011).
[19] J. D. Bekenstein, Black holes and entropy, Phys. Rev. D **7**, 2333 (1973).
[20] S. Carroll, M. C. Johnson, and L. Randall, Extremal limits and black hole entropy, J. High Energy Phys. 11 (2009) 109.
[21] S. W. Hawking, G. Horowitz, and S. F. Ross, Entropy, area, and black hole pairs, Phys. Rev. D **51**, 4302 (1995).
[22] C. Teitelboim, Action and entropy of extreme and non-extreme black holes, Phys. Rev. D **51**, 4315 (1995).
[23] A. Zee, *Quantum Field Theory in a Nutshell* (Princeton University Press, Princeton, 2010).
[24] A. Edery and N. Graham, Radiatively induced symmetry breaking and the conformally coupled magnetic monopole in AdS space, J. High Energy Phys. 11 (2013) 109.